

## Evolution of the dust/gas environment around Herbig Ae/Be stars

Tie Liu<sup>1</sup>, Huawei Zhang<sup>1</sup>, Yuefang Wu<sup>1</sup>, Sheng-Li Qin<sup>2</sup>, Martin Miller<sup>2</sup>

Received \_\_\_\_\_; accepted \_\_\_\_\_

Accepted to ApJ

---

<sup>1</sup>Department of Astronomy, Peking University, 100871, Beijing China; liutiepku@gmail.com

<sup>2</sup>I. Physikalisches Institut, Universität zu Köln, Zùlpicher Str. 77, 50937 Köln, Germany

## ABSTRACT

With the KOSMA 3-m telescope, 54 Herbig Ae/Be stars were surveyed in CO and  $^{13}\text{CO}$  emission lines. The properties of the stars and their circumstellar environments are studied by fitting the SEDs. The mean line width of  $^{13}\text{CO}$  (2-1) lines of this sample is  $1.87 \text{ km s}^{-1}$ . The average column density of  $\text{H}_2$  is found to be  $4.9 \times 10^{21} \text{ cm}^{-2}$  for the stars younger than  $10^6 \text{ yr}$ , while drops to  $2.5 \times 10^{21} \text{ cm}^{-2}$  for those older than  $10^6 \text{ yr}$ . No significant difference is found among the SEDs of Herbig Ae stars and Herbig Be stars at the same age. The infrared excess decreases with age. The envelope masses and the envelope accretion rates decrease with age after  $10^5 \text{ yr}$ . The average disk mass of the sample is  $3.3 \times 10^{-2} M_{\odot}$ . The disk accretion rate decreases more slowly than the envelope accretion rate. A strong correlation between the CO line intensity and the envelope mass is found.

*Subject headings:* Massive core:pre-main sequence-ISM: molecular-ISM: kinematics and dynamics-ISM: jets and outflows-stars: formation

## 1. Introduction

Although significant number of astrophysical processes such as outflow, inflow, disk, rotation have been observed towards high-mass star formation regions, it is still unclear whether high-mass stars form in the same way as low-mass counterparts. Thus detail studies of the circumstellar environment of young high-mass stars are especially important to understand their formation and evolution processes. However, most of high-mass stars are far away from us and deeply embedded in the clouds, which add to the difficulties of detailed studies. Intermediate-mass ( $3-8 M_{\odot}$ ) pre-main-sequence Herbig Ae/Be stars are visible at optical and infrared wavelengths which share similar circumstellar properties with massive stars, therefore will provide clues in understanding the circumstellar structure of high-mass young stars. Additionally, since Herbig Ae (HAe) stars are the precursors of vega-type systems, investigations of their circumstellar environment are also important for planet formation studies.

Herbig Ae/Be stars are still located in molecular clouds. More and more observational evidences and detailed modeling of the spectral energy distributions (SEDs) strongly suggest the presence of circumstellar disks around Herbig Ae/Be stars (Hillenbrand et al. 1992; Chiang et al. 2001; Dominik et al. 2003). To probe their surrounding gas properties especially to investigate the outer part of the disk and determine the mass and grain properties, millimeter observations are needed (Alonso-Albi et al. 2009). Recently, a handful of disks around Herbig Ae/Be stars have been spatially and spectrally resolved by optical and infrared (Boccaletti 2003; Eisner 2004; Monnier et al. 2008; Murakawa 2010; Perrin et al. 2006; Okamoto et al. 2009), as well as millimeter and sub-millimeter interferometric observations (Alonso-Albi et al. 2009; Fuente et al. 2006; Hamidouche 2010; Matthews et al. 2007; Öberg et al. 2010; Schreyer et al. 2008; Wang et al. 2008). However, the number of disks well studied at millimeter and sub-millimeter wavelengths is still very small, and more samples are needed. In addition, we now have more multi-wavelength datasets, including long-wavelength bands, than what were available for

previous studies, enabling us to model their detail structures including star-disk-envelope.

In this paper, we report the results from a survey towards 54 Herbig Ae/Be stars using the KOSMA 3-m telescope in CO and  $^{13}\text{CO}$  emission lines. Together with SED modeling, we investigate the properties of the circumstellar environment around these Herbig Ae/Be stars and explore their evolution. Our studies also provide a sample of Herbig Ae/Be stars surrounded by rich dust/gas, which are ideal for further higher spatial resolution observations by interferometers at millimeter and sub-millimeter wavelengths. The next section is about sample selection, and Section 3 describes the observation. The basic results are presented in Section 4, and more detailed discussions are given in Section 5. In section 6, a summary is present.

## 2. Sample

In order to collect a complete sample, we surveyed 54 Herbig Ae/Be stars from Thé et al. (1994) with declination  $\delta > -20^\circ$  which are accessible to KOSMA telescope. These sources cover a large age range from  $10^4$  yr to  $10^7$  yr, which are very useful to study the evolution of Herbig Ae/Be stars and their circumstellar environments. The basic parameters of these stars are listed in Table 1. The distances and spectral types of these stars are mainly obtained from Thé et al. (1994) and Manoj et al. (2006), and completed with the help of the SIMBAD database, operated at CDS, Strasbourg, France. There are 27 Ae stars, 24 Be stars and 3 Fe stars in this sample. The masses of 40 sources are obtained from Manoj et al. (2006). The effective temperatures are assigned from the spectral types and listed in the seventh column of Table 1.

## 3. Observations

The single-point survey observations in  $^{12}\text{CO}$  (2-1),  $^{12}\text{CO}$  (3-2),  $^{13}\text{CO}$  (2-1) and  $^{13}\text{CO}$  (3-2) were carried out between January and February 2010 using the KOSMA 3-m telescope at

Gornergrat, Switzerland. The medium and variable resolution acousto optical spectrometers with bandwidth of 300 and 655-1100 MHz at 230 and 345 GHz were used as backends. The spectral resolutions were 0.22 km/s and 0.29 km/s for 230 and 345 GHz, respectively. The beam width at 230 and 345 GHz were 130'' and 82'', respectively. Dual channel SIS receiver for 230/345 GHz is used for frontend, with the typical system temperatures of 120/150 K for 230/345 GHz, respectively. The forward efficiency  $F_{eff}$  was 0.93 and the corresponding main beam efficiencies  $B_{eff}$  were 0.68 and 0.72 at 230 and 345 GHz, respectively. Pointing was frequently checked on planets and was better than 10''. The integration time for each source was about 8 seconds using the total power observation mode. For the data analysis, the GILDAS software package including CLASS and GREG was employed (Guilloteau & Lucas 2000).

## 4. Results

### 4.1. Survey results

All of the sample sources were surveyed in  $^{12}\text{CO}$  (2-1) and  $^{12}\text{CO}$  (3-2) lines which have been successfully detected towards 41 out of the 54 sources. However, due to the bad weather, only 28 of the 41 sources were surveyed in  $^{13}\text{CO}$  (2-1) and  $^{13}\text{CO}$  (3-2). Fig. 1 and Fig. 2 presents the spectra of all the 54 sources. The red and green lines represent  $^{12}\text{CO}$  (2-1) and  $^{13}\text{CO}$  (2-1), respectively. For the sources not surveyed in  $^{13}\text{CO}$  emission, only  $^{12}\text{CO}$  (2-1) spectra are presented.

For the 41 sources successfully detected in  $^{12}\text{CO}$  emission, we fitted these observed lines with a Gaussian function and present the fitting parameters including the  $V_{LSR}$ , line width (FWHM) and antenna temperature  $T_A^*$  in Table 2. The systematic velocities of each source are obtained by averaging the  $V_{LSR}$  of  $^{13}\text{CO}$  (2-1) and  $^{13}\text{CO}$  (3-2) lines if available. For the sources not surveyed in  $^{13}\text{CO}$  emission, the systematic velocities are obtained by averaging the  $V_{LSR}$  of  $^{12}\text{CO}$  (2-1)

and  $^{12}\text{CO}$  (3-2) lines. The derived systematic velocities are listed in the [col. 2] of Table 3. The spectral profiles of these sources show rich properties. Together with  $^{13}\text{CO}$  (2-1) lines, the profiles of  $^{12}\text{CO}$  (2-1) lines are identified and listed in the last column of Table 2. There are 11 sources having multiple components; 3 sources having flat tops; 5 sources showing red asymmetry profile and 5 sources showing blue asymmetry profile. Additionally, 2 sources are identified as blue profile, 1 source as red profile, and 1 source shows self-absorption.

The intensity ratios of  $^{12}\text{CO}$  (2-1) and  $^{13}\text{CO}$  (2-1) are derived and listed in the [col. 3] of Table 3. The  $^{12}\text{CO}$  (2-1) optical depth can be obtained from the comparison of the observed  $^{12}\text{CO}$  (2-1) and  $^{13}\text{CO}$  (2-1) antenna temperature, assuming  $[^{12}\text{CO}]/[^{13}\text{CO}]=89$ . The  $^{12}\text{CO}$  (2-1) lines are found to be always optically thick with an average optical depth of 26.6. Since the  $^{12}\text{CO}$  is optically thick, the excitation temperature  $T_{ex}$  can be obtained according to Garden et al. (1991):

$$T_r = \frac{T_A^*}{\eta_b} = \frac{h\nu}{k} \left[ \frac{1}{\exp(h\nu/kT_{ex}) - 1} \frac{1}{\exp(h\nu/kT_{bg}) - 1} \right] \times f_\nu \quad (1)$$

where  $T_{bg} = 2.73 \text{ K}$  is the temperature of the cosmic background radiation,  $f_\nu = f_{82} = \frac{\Theta_s^2}{\Theta_s^2 + 82^2}$ ,  $f_\nu = f_{130} = \frac{\Theta_s^2}{\Theta_s^2 + 130^2}$  are the beam-filling factors of the  $^{12}\text{CO}$  (3-2) and the  $^{12}\text{CO}$  (2-1), respectively. The source size  $\Theta_s$  and the excitation temperature  $T_{ex}$  can be calculated simultaneously from equ (1) using  $^{12}\text{CO}$  (2-1) and  $^{12}\text{CO}$  (3-2) data together. To calculate the line ratios  $R_{3,2}$  of the  $^{12}\text{CO}$  (3-2) and the  $^{12}\text{CO}$  (2-1), beam filling factor should be taken into account. The corrected line ratios  $R_{3,2}$  can be obtained from:  $R_{3,2} = f_{82,130} \cdot \frac{\int T_A(^{12}\text{CO}(3-2))d\nu}{\int T_A(^{12}\text{CO}(2-1))d\nu}$ , where  $f_{82,130} = \frac{1+(82/\Theta_s)^2}{1+(130/\Theta_s)^2}$  and  $\Theta_s$  is the source size.

Assuming the  $^{13}\text{CO}$  (2-1) is optically thin, the optical depth and column density of the  $^{13}\text{CO}$  can be straightforwardly obtained under local thermal equilibrium (LTE) assumption. With the abundance ratio  $[\text{H}_2]/[^{13}\text{CO}]=8.9 \times 10^5$ , the column density of  $\text{H}_2$  also can be calculated. For these sources which have not been surveyed with the  $^{13}\text{CO}$ , the column densities of  $\text{H}_2$  are firstly obtained from the  $^{12}\text{CO}$  (2-1) lines under the assumption that the  $^{12}\text{CO}$  (2-1) emission is optically thin and  $[\text{H}_2]/[^{12}\text{CO}]=10^4$ , and then multiplied by an optical depth correction factor

$C_\tau = \tau/(1 - e^{-\tau})$ . The optical depths of the  $^{12}\text{CO}$  (2-1) for those sources not surveyed in the  $^{13}\text{CO}$  emission are assigned as 26.6, the average value obtained above. All the results are collected in Table 3.

## 4.2. The SED

We have compiled the SEDs for 53 sources in the sample except MWC 614, which has not enough data to use for modeling. The optical (UBV) data are from Manoj et al. (2006), JHK fluxes from the 2MASS All-Sky Catalog of Point Sources, IRAC and MIPS data from Harvey et al. (2007); Gutermuth et al. (2009), IRAS data from the IRAS catalogue of Point Sources, MSX data from MSX6C Infrared Point Source Catalog, AKAIR data from AKARI/IRC mid-IR all-sky Survey and AKARI/FIS All-Sky Survey Point Source Catalogues, SCUBA 450  $\mu\text{m}$  and 850  $\mu\text{m}$  submillimeter data from Di Francesco et al. (2008), 1.3 mm continuum data from Henning et al. (1994). We also collected sub-mm and mm data for some sources from Mannings et al. (1994), Acke et al. (2004), Di Francesco et al. (1997), and Alonso-Albi et al. (2009). Although not all the sources have data at all the wavelength bands, there are still enough data for each source to be used for fitting the SED.

The SEDs are then modeled using the online 2D-radiative transfer tool developed by Robitaille et al. (2006), which has been successfully tested by Robitaille et al. (2007), on a sample of low-mass YSOs and by Grave & Kumar (2009) on high-mass protostars. The geometry in the models consists of a central star surrounded by a flared accretion disk, a rotationally flattened infalling envelope and bipolar cavities. The SED fitting tool uses 200,000 YSO model SEDs (20,000 sets of physical parameters and 10 viewing angles). The distance and visual extinction are the only two input parameters in the fitting process. During the fitting process, all the model SEDs in the grid are compared with the observed data, and the model SEDs that fit a source well can be picked out within a specified limit on  $\chi^2$ . For each source, a minimum of three data points

that are of good quality are required by the SED model tool. In our sample, all the 53 sources have at least ten such data points, spreading over the wavelength region of 0.3 to 2600  $\mu\text{m}$ , which can well constraint the models with least standard deviations (Robitaille et al. 2007). However, the two input parameters of the distance and visual extinction are far from fixed, which lead to the degeneracy of the models. In our cases, we assumed 30% uncertainty for each of the distances obtained from literatures, and varied the visual extinction  $A_v$  from 0 to 30. Although the best fit model has the least  $\chi^2$  value, it may not actually represent the data very well (Grave & Kumar 2009). In order to find a representative set of values for each source, all the models are accepted and analyzed, which satisfy the criterion of  $\chi^2 - \chi_{best}^2 < 3 \times n_{data}$ , where  $n_{data}$  is the number of the data points. Fig. 3 and Fig. 4 shows the observed SEDs and model SEDs with  $\chi^2 - \chi_{best}^2 < 3 \times n_{data}$ . Following Grave & Kumar (2009), a weighted mean and standard deviation are derived for all the parameters of each source, with the weights being the inverse of the  $\chi^2$  of each model. All the parameters derived are listed in Table 4. The various columns in Table 4. are as follows: [col. 1] name of the source; [col. 2] visual extinction; [col. 3] age of the star; [col. 4] mass of the star; [col. 5] radius of the star; [col. 6] total luminosity of the star; [col. 7] temperature of the star; [col. 8] envelope mass; [col. 9] envelope accretion rate; [col. 10] disk mass ; [col. 11] disk inclination angle; [col. 12] outer radius of the disk; [col. 13] disk accretion rate.

## 5. Discussion

### 5.1. The CO emission

The mean line width of the  $^{13}\text{CO}(2-1)$  lines of this sample is 1.87  $\text{km s}^{-1}$  with a standard deviation of 0.66  $\text{km s}^{-1}$ . This line width is similar to that of intermediate-mass star formation regions ( $\sim 2 \text{ km s}^{-1}$ ) (Sun et al. 2006), larger than that of low-mass star formation regions (1.3  $\text{km s}^{-1}$ ) (Myers, Linke & Benson 1983), but much smaller than that of high-mass star formation regions associated with IRAS sources (3.09  $\text{km s}^{-1}$ ) (Wang et al. 2009; Wu et al. 2003).



The average column density of  $H_2$  is found to be  $4.9 \times 10^{21} \text{ cm}^{-2}$  before  $10^6$  yr, while drops to  $2.5 \times 10^{21} \text{ cm}^{-2}$  after  $10^6$  yr. As shown in the left panel of Fig.5, the optical depth of the  $^{12}\text{CO}(2-1)$  ranges from 7.5 to 54 with an average value of 27.7 before  $10^6$  yr, but the optical depth drops below 26.6 (the average value in this sample) after  $10^6$  yr, with an average value of 22.5. The excited temperature of CO ranges from 4.3 K to 33 K, with an average of 13.8 K. As shown in the right panel of Fig.5, a decreased trend is found for the excited temperature with age. The decrease of the optical depth and excitation temperature with age may be due to the different gas dispersion mechanisms in which most of gas should be dispersed by outflows and stellar winds at the early evolutionary stage of the stars, and UV radiation and photodissociation play an important role in further gas dispersion as the stars evolve (Fuente et al. 2002). Therefore only less dense molecular gas with low excitation temperature existed in outer envelope of late-type stars is observed at millimeter and submillimeter wavelengths.

## 5.2. The properties of the stars

The ages of the sample stars spread from  $10^3$  yr to  $10^7$  yr. About 40% sample stars are younger than  $10^6$  yr, and the others are older than  $10^6$  yr. The average mass of the stars is  $3.9 \pm 2.2 M_{\odot}$ . In the left panel of Fig.6, we compare the masses derived from SED fitting to those obtained from Manoj et al. (2006). The masses ( $M_{mod}$ ) from the SED modeling are well coincident with the masses ( $M_{lit}$ ) obtained from literatures with a relationship of  $M_{mod} = M_{lit} \pm 0.44$ , where the correlation coefficient  $r=0.64$ . Although the masses derived from the SED fitting seems slightly higher than those from literatures, they are found to agree with each other better than  $\pm 0.3$  orders of magnitude. We also compare the effective temperatures of the stars obtained from SED fitting to those corresponding to the spectral types. We find the agreement of the effective temperatures obtained from the two independent methods for 80% of the sample sources is better than  $\pm 0.3$  orders of magnitude. The average effective temperature of the sample stars is

$(1.1 \pm 0.6) \times 10^4$  K. As shown in Fig.7, the mass-luminosity function of the sample stars is found to be  $\text{Log}(L_*/L_\odot) = (3.08 \pm 0.17)\text{Log}(M_*/M_\odot) + (0.48 \pm 0.10)$ , with the correlation coefficient  $r=0.93$ .

### 5.3. The evolution of the SED

Meeus et al. (2001) proposed that the SEDs of Herbig Ae/Be stars can be divided into two groups based on the different mid-infrared excesses: Group I sources with strong mid-infrared flux while Group II sources with weaker infrared excesses. Acke et al. (2005) found most HAe stars belong to Group I and most HBe stars belong to Group II. However, there may be an evolutionary link between Group I and Group II sources. We display the SEDs of the HAe stars and HBe stars in our sample in Fig.3 and Fig.4 ordered by age (age increases from top-left to bottom-right panel), respectively. Firstly, we find no significant difference among the SEDs of HAe stars and HBe stars at the same age; secondly, it is clearly to see the infrared excess decreases with age for both HAe stars and HBe stars. The dashed lines show the SEDs of the stellar photosphere, including the effect of foreground extinction, from the best-fitting model (Robitaille et al. 2006). As shown in the second column of Table 4, the interstellar extinctions  $A_v$  range from 0 to 12 mag in our sample from the SED modeling. We find at early ages ( $< 10^6$  yr), the optical and near-infrared fluxes of most of the HAe and HBe stars can not be simply fitted by a stellar photosphere with interstellar extinction, while the older ones ( $> 10^6$  yr) can be well fitted, indicating huge amounts of circumstellar dust/gas exist at early ages, which causes large extinction and infrared excess. The shortest wavelength at which infrared excess is recognizable is around  $2 \mu\text{m}$ . At early ages, the excess at sub-mm/mm regions is also very significant and HAe stars seem to have stronger sub-mm/mm excess than HBe stars at the same age.

#### 5.4. The circumstellar envelopes and the disks

The left panel of Fig.8 gives the number distribution of the envelope mass and presents the envelope mass as function of stellar age. There is no difference in the distribution of the envelope masses between HAe stars and HBe stars. The envelope masses of the HAe and HBe stars are larger than  $10^{-2} M_{\odot}$  before  $10^6$  yr, but smaller than  $10^{-2} M_{\odot}$  after  $10^6$  yr. The envelope masses decrease with age after  $10^5$  yr following the relationship:  $\text{Log}(M_{\text{env}}/M_{\odot}) = (-4.0 \pm 0.5)\text{Log}(t/\text{yr}) + (22 \pm 3.4)$ , with the correlation coefficient  $r=0.74$ . The number distribution of the envelope accretion rate and the envelope accretion rate as function of stellar age are presented in the right panel of Fig.8. The average envelope accretion rate for the Herbig Ae/Be stars younger than  $10^6$  yr is  $2.5 \times 10^{-5} M_{\odot} \cdot \text{yr}^{-1}$ . The envelope accretion rate drops below  $10^{-6} M_{\odot} \cdot \text{yr}^{-1}$  after  $10^6$  yr, and 25 sources older than  $10^6$  yr have zero envelope accretion rate, which means those sources can be explained by disk-only sources without infalling envelope. We also find the envelope accretion rate decrease with age after  $10^5$  yr following the relationship:  $\text{Log}(\dot{M}_{\text{env}}/M_{\odot} \cdot \text{yr}^{-1}) = (-2.4 \pm 0.5)\text{Log}(t/\text{yr}) + (8.2 \pm 3.0)$ , with the correlation coefficient  $r=0.72$ .

From the left panel of Fig.9, it can be seen the disk masses locate at a narrow range from  $10^{-3} M_{\odot}$  to  $10^{-1} M_{\odot}$  if neglecting the three points with extremely small disk mass. The average disk mass is  $3.3 \times 10^{-2} M_{\odot}$ , and the maximum one is  $0.26 M_{\odot}$  from AS 447. No obvious evolutionary pattern is found towards the disk masses. The right panel of Fig. 9 shows the disk accretion rate as function of stellar age. The average disk accretion rate is  $5 \times 10^{-8} M_{\odot} \cdot \text{yr}^{-1}$ . An average disk accretion rate of  $3.6 \times 10^{-7} M_{\odot} \cdot \text{yr}^{-1}$  is found for those sources younger than  $10^6$  yr, which is much lower than the corresponding envelope accretion rate, suggesting the envelopes dominate the accretion at early stages of star formation. However, after  $10^6$  yr, the envelope accretion halts ( $\dot{M}_{\text{env}} \sim 0$ ), while the disk accretion rate remains  $\sim 1.6 \times 10^{-8} M_{\odot} \cdot \text{yr}^{-1}$ . Additionally, the disk accretion rate decreases with age following the

relationship:  $\text{Log}(\dot{M}_{\text{disk}}/M_{\odot} \cdot \text{yr}^{-1}) = (-0.6 \pm 0.1)\text{Log}(t/\text{yr}) + (3.5 \pm 0.7)$ , with the correlation coefficient  $r=0.6$ , nevertheless the disk accretion rate decreases much more slowly than the envelope accretion rate.

### 5.5. The relationship between CO gas and the envelope

Fig.10 presents the line intensity of the  $^{12}\text{CO}$  (2-1) and  $^{12}\text{CO}$  (3-2) as function of stellar age. It can be seen the CO line intensities of most of the sources younger than  $10^6$  yr are larger than  $10 \text{ K km s}^{-1}$ , and drop below  $10 \text{ K km s}^{-1}$  after  $10^6$  yr. The evolution behaviors of CO line intensity is very similar to that of envelope (see Fig.8), suggesting possible co-evolution between the envelope and the CO gas. We plot the line intensity of the  $^{12}\text{CO}$  (2-1) and the  $^{12}\text{CO}$  (3-2) as function of envelope mass in Fig.11. Exclude those data with line intensities smaller than  $1 \text{ K km s}^{-1}$ , which have low signal-to-noise level or no detection of CO emission, the CO line intensity is well correlated with the envelope mass. For  $^{12}\text{CO}$  (2-1), the relationship can be fitted by a power-law:  $\text{Log}(I_{\text{CO}(2-1)}/\text{K km s}^{-1}) = (0.076 \pm 0.017)\text{Log}(M_{\text{env}}/M_{\odot}) + (1.129 \pm 0.052)$ , where the correlation coefficient  $r=0.64$ . For  $^{12}\text{CO}$ (3-2), the relationship can also be fitted by a power-law:  $\text{Log}(I_{\text{CO}(3-2)}/\text{K km s}^{-1}) = (0.098 \pm 0.019)\text{Log}(M_{\text{env}}/M_{\odot}) + (1.037 \pm 0.066)$ , with a correlation coefficient  $r=0.64$ . It seems that CO gas is associated with the envelopes.

## 6. Summary

We have surveyed 54 Herbig Ae/Be stars using the KOSMA 3-m telescope in the CO and the  $^{13}\text{CO}$  emission lines. Together with SED modeling, we have investigated the properties of the circumstellar environments around those Herbig Ae/Be stars and explored their evolutionary characteristics. The main findings of this paper are as below:

- (1). We have successfully detected CO emission towards 41 out of the 54 sources, and 28 of

the 41 sources were surveyed in  $^{13}\text{CO}$  (2-1) and  $^{13}\text{CO}$  (3-2). The mean line width of the  $^{13}\text{CO}$  (2-1) line width of this sample is  $1.87 \text{ km s}^{-1}$ , which is similar to that of intermediate-mass star formation regions ( $\sim 2 \text{ km s}^{-1}$ ). The average column density of  $\text{H}_2$  is found to be  $4.9 \times 10^{21} \text{ cm}^{-2}$  before  $10^6 \text{ yr}$ , while drops to  $2.5 \times 10^{21} \text{ cm}^{-2}$  after  $10^6 \text{ yr}$ .

(2).The SEDs of 53 sources are compiled and modeled using the online 2D-radiative transfer tool. From the SED fitting, we find 40% sample stars are younger than  $10^6 \text{ yr}$ , and the others are older than  $10^6 \text{ yr}$ . The average mass of the stars is  $3.9 \pm 2.2 M_{\odot}$ . The mass-luminosity function of the sample stars can be described as  $\text{Log}(L_*/L_{\odot}) = (3.08 \pm 0.17)\text{Log}(M_*/M_{\odot}) + (0.48 \pm 0.10)$ .

(3).We find no significant difference among the SEDs of HAe stars and HBe stars at the same age and the infrared excess decreases with age for both HAe stars and HBe stars.

(4).The envelop masses decrease with age after  $10^5 \text{ yr}$ . The average envelop accretion rate for the Herbig Ae/Be stars younger than  $10^6 \text{ yr}$  is  $2.5 \times 10^{-5} M_{\odot}\cdot\text{yr}^{-1}$  and drops below  $10^{-6} M_{\odot}\cdot\text{yr}^{-1}$  after  $10^6 \text{ yr}$ . In our sample 25 sources older than  $10^6 \text{ yr}$  have zero envelop accretion rate. The average disk mass of the sample is  $3.3 \times 10^{-2} M_{\odot}$ . The disk accretion rate decreases with age, but more slowly than the envelope accretion rate.

(5).The CO line intensities of most of the sources younger than  $10^6 \text{ yr}$  are larger than  $10 \text{ K km s}^{-1}$ , and drop below  $10 \text{ K km s}^{-1}$  after  $10^6 \text{ yr}$ . The CO line intensity is well correlated with the envelope mass, suggesting possible co-evolution between the envelope and the CO gas.

### Acknowledgment

This work was supported by the NSFC under grants No. 11073003, 10733030, and 10873019, and by the National key Basic Research Program (NKBRP) No. 2007CB815403.

## REFERENCES

- Acke, B., van den Ancker, M. E., Dullemond, C. P., van Boekel, R., Waters, L. B. F. M., 2004, A&A, 422, 621
- Acke, B., van den Ancker, M. E., & Dullemond, C. P., 2005, A&A, 436, 209
- Alonso-Albi, T., Fuente, A., Bachiller, R., Neri, R., Planesas, P., Testi, L., 2008, ApJ, 680, 1289
- Alonso-Albi, T., Fuente, A., Bachiller, R., Neri, R., Planesas, P., Testi, L., Berné, O., Joblin, C., 2009, A&A, 497, 117
- Boccaletti, A., Augereau, J.-C., Marchis, F., Hahn, J., 2003, ApJ, 585, 494
- Chiang, E. I., Joungh, M. K., Creech-Eakman, M. J., Qi, C., Kessler, J. E., Blake, G. A., van Dishoeck, E. F., 2001, ApJ, 547, 1077
- Di Francesco, James., Evans, Neal J., II., Harvey, Paul M., Mundy, Lee G., Guilloteau, Stephane., Chandler, Claire J., 1997, ApJ, 482, 433
- Di Francesco, James., Johnstone, Doug., Kirk, Helen., MacKenzie, Todd., Ledwosinska, Elizabeth., 2008, ApJS, 175, 277
- Dominik, C., Dullemond, C. P., Waters, L. B. F. M., Natta, A., 2003, ASPC, 287, 313
- Eisner, J. A., Lane, B. F., Hillenbrand, L. A., Akeson, R. L., Sargent, A. I., 2004, ApJ, 613, 1049
- Fuente, A., Martín-Pintado, J., Bachiller, R., Rodríguez-Franco, A., Palla, F., 2002, A&A, 387, 977
- Fuente, A., Rodríguez-Franco, A., Testi, L., Natta, A., Bachiller, R., Neri, R., 2003, ApJ, 598, L39
- Fuente, A., Alonso-Albi, T., Bachiller, R., Natta, A., Testi, L., Neri, R., Planesas, P., 2006, ApJ, 649, L119
- Garden, R. P., Hayashi, M., Hasegawa, T., Gatley, I., Kaifu, N., 1991, ApJ, 374, 540
- Grave J. M. C. & Kumar M. S. N., 2009, A&A, 498, 147

- Guilloteau, S. & Lucas, R., 2000, in *Astronomical Society of the Pacific Conference Series*, Vol. 217, Imaging at Radio through Submillimeter Wavelengths, ed. J. G. Mangum & S. J. E. Radford, 299
- Gutermuth, R. A., Megeath, S. T., Myers, P. C., Allen, L. E., Pipher, J. L., Fazio, G. G., 2009, *ApJS*, 184, 18
- Hamidouche, M., 2010, *ApJ*, 722, 204
- Harvey, Paul; Merín, Bruno; Huard, Tracy L.; Rebull, Luisa M.; Chapman, Nicholas; Evans, Neal J., II; Myers, Philip C., 2007, *ApJ*, 663, 1149
- Henning, Th., Launhardt, R., Steinacker, J., Thamm, E., 1994, *A&A*, 291, 546
- Hillenbrand, Lynne A., Strom, Stephen E., Vrba, Frederick J., Keene, Jocelyn., 1992, *ApJ*, 397, 613
- Manoj, P., Bhatt, H. C., Maheswar, G., Muneer, S., 2006, *ApJ*, 653, 657
- Mannings, V., 1994, *MNRAS*, 271, 587
- Matthews, B. C., Graham, J. R., Perrin, M. D., Kalas, P., 2007, *ApJ*, 671, 483
- Meeus, G., Waters, L. B. F. M., Bouwman, J., van den Ancker, M. E., Waelkens, C., Malfait, K., 2006, *A&A*, 365, 476
- Monnier, J. D., Tannirkulam, A., Tuthill, P. G., Ireland, M., Cohen, R., Danchi, W. C., Baron, F., 2008, *ApJ*, 681, L97
- Murakawa, K., 2010, *A&A*, 522, 46
- Myers, P. C., Linke, R. A., & Benson, P. J., 1983, *ApJ*, 264, 517
- Öberg, K. I., et al., 2010, *ApJ*, 720, 480
- Okamoto, Y. K., et al., 2009, *ApJ*, 706, 665
- Perrin, M. D., Schneider, G., Duchene, G., Pinte, C., Grady, C. A., Wisniewski, J. P., Hines, D. C., 2009, *ApJ*, 707, L132

- Robitaille T. P., Whitney B. A., Indebetouw R., Wood K., & Denzmore P., 2006, *ApJS*, 167, 256
- Robitaille T. P., Whitney B. A., Indebetouw R., and Wood K., 2007, *ApJS*, 169, 328
- Schreyer, K., et al., 2008, *A&A*, 491, 821
- Sun, K., Kramer, C., Ossenkopf, V., Bensch, F., Stutzki, J., Miller, M., *A&A*, 451, 539
- Thé, P. S., de Winter, D., & Perez, M. R., 1994, *A&AS*, 104, 315
- Wang, K., Wu, Y. F., Ran, L., Yu, W. T., Miller, M., 2009, *A&A*, 507, 369
- Wang, S., Looney, L. W., Brandner, W., Close, L. M., 2008, *ApJ*, 673, 315
- Wu, Y., Wang, J., & Wu, J., 2003, *Chin. Phys. Letter*, 20, 1409



Table 1. Parameters of all the Herbig Ae/Be stars surveyed

Name	$\alpha$ (J2000) (h m s)	$\delta$ (J2000) ( $^{\circ}$ $'$ $''$ )	Distance (pc)	Spectral Type	$M_*$ $M_{\odot}$	$\log(T_{eff})$ $\log(K)$
MacC H12	00 07 02.6	65 38 38.2	850	A5 D		3.91
LkHA 198 / V633cas <sup>b</sup>	00 11 26.0	58 49 29.1	600	B9 D	4.25	4.02
Vx Cas	00 31 30.7	61 58 51.0	760	A0 D	3	3.98
RNO 6	02 16 30.1	55 22 57.0	1600	B3 D	5.99	4.27
IP Per	03 40 47.0	32 31 53.7	350	A6 D	2	3.92
XY Per	03 49 36.2	38 58 55.5	160	A2IIv+ C	2	3.91
V892 Tau <sup>a,b</sup>	04 18 40.6	28 19 15.5	160	B8 D	>5.11	4.08
AB Aur <sup>a,b</sup>	04 55 45.8	30 33 04.3	144	A0Vpe C	2.77	3.97
MWC 480 <sup>a,b</sup>	04 58 46.3	29 50 37.0	131	A3Ve D	1.99	3.94
HD 35929	05 27 42.8	-08 19 38.4	345	F2III D	3.41	3.84
HD 36112	05 30 27.5	25 19 57.1	205	A5 IVe	2.17	3.91
HD 245185	05 35 09.6	10 01 51.5	400	A1 D	2.07	3.97
T Ori <sup>a</sup>	05 35 50.4	-05 28 34.9	460	A3V C	3.34	3.98
CQ Tau <sup>a,b</sup>	05 35 58.5	24 44 54.1	100	F3 D	1.5	3.83
V380 Ori	05 36 25.4	-06 42 57.7	510	A1e D	>4.93	3.97
V586 Ori	05 36 59.3	-06 09 16.4	510	A2V C	3	3.98
BF Ori	05 37 13.3	-06 35 00.6	430	A5II-IIIev C	2.5	3.95
HD37411	05 38 14.5	-05 25 13.3		B9Ve		4.02
Haro 13A	05 38 18.2	-07 02 25.9	460	Be		
V599 Ori	05 38 58.6	-07 16 45.6	360	A5 D		3.91
RR Tau	05 39 30.5	26 22 27.0	800	A2II-IIIe C	4.26	3.98
V350 Ori	05 40 11.8	-09 42 11.1	460	A1 D	2.22	3.97
MWC 789	06 01 60.0	16 30 56.7	700	B9 D	4.13	4.02
LkHA 208	06 07 49.5	18 39 26.5	1000	A7 D	3.24	3.89
LkHA 339	06 10 57.8	-06 14 37	830	A1 D	3.18	3.97
LkHA 215 <sup>b</sup>	06 32 41.8	10 09 33.6	800	B6 D	>5.43	4.15
R Mon <sup>a,b</sup>	06 39 10	08 44 09.7	800	B0	>5.11	4.08
V590 Mon	06 40 44.6	09 48 02.1	800	B7 D	<3.35	4.11
GU CMa	07 01 49.5	-11 18 03.3		B2Vne C		4.34
HD 141569 <sup>a</sup>	15 49 57.7	-03 55 16.3	99	A0Ve D	2.18	3.98
VV Ser <sup>a,b</sup>	18 28 47.9	00 08 39.8	330	B6 D	>5.43	4.15

Table 1—Continued

Name	$\alpha$ (J2000) (h m s)	$\delta$ (J2000) ( $^{\circ}$ $'$ $''$ )	Distance (pc)	Spectral Type	$M_*$ $M_{\odot}$	$\log(T_{eff})$ $\log(K)$
MWC 300	18 29 25.7	-06 04 37.1	650	Bpe D		
AS 310	18 33 27	-04 58 06	2500	B1	>6	4.4
MWC 614	19 11 04.3	21 11 26				
Par 21	19 29 00.8	09 38 46.7	300	A5e		3.91
V1295 Aql <sup>a</sup>	20 03 02.5	05 44 16.7	290	A2IVe D	3.03	3.95
V1685 Cyg <sup>a</sup>	20 20 28.2	41 21 51.6	980	B3 D	>5.99	4.27
Par 22	20 24 29.5	42 14 03.7		A5 eV		3.91
PV Cep <sup>b</sup>	20 45 53.9	67 57 38.9	500	A5 D		3.91
AS 442 <sup>a</sup>	20 47 37.5	43 47 25.0	826	B9 D		4.02
LkHA 134	20 48 04.8	43 47 25.8	700	B2 D	>6	4.34
HD 200775 <sup>a</sup>	21 01 36.9	68 09 47.8	429	B2 Ve C	>5.99	4.27
LkHA 324	21 03 54.2	50 15 10.2	780	B8 D	>5.11	4.08
HD 203024	21 16 03	68 54 52.1		A D		
V645 Cyg	21 39 58.2	50 14 21.2	3500	A0 D	>4.94	3.98
LkHA 234	21 43 02.3	66 06 29	1250	B5 Vev	>5.29	4.11
AS 477 / BD 46	21 52 34.1	47 13 43.6	1200	B9.5Ve C	>4.94	3.98
LkHA 257	21 54 18.8	47 12 09.7	900	B5 D		4.19
BH Cep	22 01 42.9	69 44 36.5	450	F5IV C	1.73	3.81
SV Cep	22 21 33.2	73 40 27.1	440	A0 D	2.5	3.98
V375 Lac	22 34 41	40 40 04.5	880	A4 D	3.19	3.93
IL Cep	22 53 15.6	62 08 45	725	B2IV-Vne C		4.34
MWC 1080 <sup>a,b</sup>	23 17 25.6	60 50 43.6	2200	B0eq D	>6	4.48
LkHA 259	23 58 41.6	66 26 12.6	890	A9 D		3.87

<sup>a</sup>Circumstellar disks detected by optical or infrared observations (Boccaletti 2003; Eisner 2004; Monnier et al. 2008; Murakawa 2010; Perrin et al. 2006; Okamoto et al. 2009).

<sup>b</sup>Circumstellar disks detected by millimeter and sub-millimeter interferometric observations (Alonso-Albi et al. 2009; Fuente et al. 2006; Hamidouche 2010; Matthews et al. 2007; Öberg et al. 2010; Schreyer et al. 2008; Wang et al. 2008).

Table 2. Observational Parameters of the lines

Name	$^{13}\text{CO}$ (2-1)			$^{13}\text{CO}$ (3-2)			CO (2-1)			CO (3-2)			Notes
	$V_{LSR}$ (km s $^{-1}$ )	FWHM (km s $^{-1}$ )	$T_A^*$ (K)	$V_{LSR}$ (km s $^{-1}$ )	FWHM (km s $^{-1}$ )	$T_A^*$ (K)	$V_{LSR}$ (km s $^{-1}$ )	FWHM (km s $^{-1}$ )	$T_A^*$ (K)	$V_{LSR}$ (km s $^{-1}$ )	FWHM (km s $^{-1}$ )	$T_A^*$ (K)	
MacC H12	$-4.82 \pm 0.02$	$1.67 \pm 0.04$	2.64	$-4.63 \pm 0.07$	$1.03 \pm 0.16$	1.57	$-5.05 \pm 0.02$	$2.30 \pm 0.03$	6.98	$-5.14 \pm 0.04$	$2.50 \pm 0.09$	7.92	flat top
LkHA 198	$-0.25 \pm 0.01$	$2.25 \pm 0.02$	3.00	$-0.06 \pm 0.03$	$1.98 \pm 0.06$	2.59	$-0.14 \pm 0.01$	$3.07 \pm 0.01$	6.84	$-0.06 \pm 0.02$	$2.67 \pm 0.05$	6.06	wings
RNO 6	$-36.20 \pm 0.02$	$1.59 \pm 0.03$	1.50	$-35.87 \pm 0.04$	$1.51 \pm 0.10$	1.41	$-36.31 \pm 0.02$	$2.34 \pm 0.04$	2.81	$-36.27 \pm 0.09$	$2.31 \pm 0.21$	2.50	flat top
XY Per	$-4.20 \pm 0.07$	$2.11 \pm 0.18$	0.47				$-4.87 \pm 0.04$	$3.28 \pm 0.09$	2.23	$-4.73 \pm 0.10$	$2.68 \pm 0.30$	2.47	red asy
V892 Tau	$7.40 \pm 0.01$	$1.33 \pm 0.02$	2.14	$6.98 \pm 0.05$	$1.49 \pm 0.15$	1.12	$7.09 \pm 0.01$	$2.92 \pm 0.03$	4.14	$6.89 \pm 0.02$	$2.31 \pm 0.05$	3.64	blue asy
AB Aur							$6.10 \pm 0.01$	$1.04 \pm 0.01$	4.70	$6.18 \pm 0.01$	$0.96 \pm 0.02$	4.96	
T Ori	$7.47 \pm 0.01$	$1.28 \pm 0.03$	4.27	$7.48 \pm 0.03$	$1.19 \pm 0.06$	8.58	$7.29 \pm 0.21$	$1.78 \pm 0.21$	13.51	$7.20 \pm 0.01$	$1.58 \pm 0.01$	24.73	three comp
	$10.83 \pm 0.12$	$2.50 \pm 0.18$	2.76	$11.15 \pm 0.25$	$1.99 \pm 0.55$	3.07	$10.42 \pm 0.21$	$3.07 \pm 0.21$	14.38	10.34	$2.73 \pm 0.03$	19.27	
	$13.13 \pm 0.16$	$2.32 \pm 0.25$	1.86	$13.34 \pm 0.62$	$2.02 \pm 0.84$	1.35	$13.30 \pm 0.21$	$3.37 \pm 0.21$	11.40	13.17	$3.42 \pm 0.04$	14.13	
V380 Ori	$6.99 \pm 0.05$	$1.35 \pm 0.11$	2.34	$6.93 \pm 0.09$	$0.82 \pm 0.17$	1.85							
	$8.95 \pm 0.03$	$2.14 \pm 0.06$	6.44	$9.02 \pm 0.05$	$2.03 \pm 0.12$	5.60	8.85	$4.01 \pm 0.02$	7.46	$8.95 \pm 0.02$	$3.40 \pm 0.05$	6.50	two comp
V586 Ori							$6.54 \pm 0.03$	$1.77 \pm 0.07$	2.18	$6.54 \pm 0.06$	$1.93 \pm 0.21$	1.70	two comp
							$8.74 \pm 0.01$	$1.42 \pm 0.02$	7.43	$8.75 \pm 0.01$	$1.31 \pm 0.03$	9.09	
BF Ori	6.59	$1.64 \pm 0.05$	2.86	$5.77 \pm 0.07$	$1.12 \pm 0.16$	2.46	$6.54 \pm 0.21$	$2.82 \pm 0.21$	6.75	$6.05 \pm 0.04$	$2.46 \pm 0.06$	6.53	three comp
	$9.17 \pm 0.09$	$1.82 \pm 0.18$	1.49				$9.14 \pm 0.21$	$2.32 \pm 0.21$	3.98	$8.77 \pm 0.05$	$2.75 \pm 0.13$	4.36	
	$10.89 \pm 0.10$	$1.22 \pm 0.24$	0.88				$10.70 \pm 0.21$	$1.56 \pm 0.21$	1.79	$10.40 \pm 0.02$	$1.22 \pm 0.08$	1.32	
Haro 13A	$5.78 \pm 0.02$	$2.10 \pm 0.05$	2.38	$5.47 \pm 0.07$	$1.01 \pm 0.19$	2.17	$5.71 \pm 0.02$	$3.62 \pm 0.02$	6.00	$5.19 \pm 0.08$	$2.92 \pm 0.07$	5.14	blue asy
V599 Ori	$5.02 \pm 0.04$	$2.40 \pm 0.12$	1.35	$5.07 \pm 0.20$	$2.73 \pm 0.53$	0.67	$5.25 \pm 0.02$	$3.51 \pm 0.03$	4.78	$4.94 \pm 0.15$	$3.49 \pm 0.11$	3.24	two comp?
	$7.18 \pm 0.05$	$1.24 \pm 0.13$	0.77										
RR Tau	$-5.40 \pm 0.02$	$1.36 \pm 0.06$	1.55	$-5.41 \pm 0.04$	$0.98 \pm 0.10$	1.14	$-5.09 \pm 0.01$	$1.83 \pm 0.02$	5.22	$-5.02 \pm 0.01$	$1.84 \pm 0.02$	6.80	
V350 Ori	$4.39 \pm 0.06$	$1.37 \pm 0.16$	0.69				$3.70 \pm 0.04$	$3.25 \pm 0.06$	1.84	$3.68 \pm 0.05$	$3.78 \pm 0.41$	1.01	blue profile

Table 2—Continued

Name	$^{13}\text{CO}$ (2-1)			$^{13}\text{CO}$ (3-2)			CO (2-1)			CO (3-2)			Notes
	$V_{LSR}$ (km s $^{-1}$ )	FWHM (km s $^{-1}$ )	$T_A^*$ (K)	$V_{LSR}$ (km s $^{-1}$ )	FWHM (km s $^{-1}$ )	$T_A^*$ (K)	$V_{LSR}$ (km s $^{-1}$ )	FWHM (km s $^{-1}$ )	$T_A^*$ (K)	$V_{LSR}$ (km s $^{-1}$ )	FWHM (km s $^{-1}$ )	$T_A^*$ (K)	
MWC 789	$2.57 \pm 0.08$	$1.80 \pm 0.20$	0.58				$2.61 \pm 0.02$	$2.01 \pm 0.04$	1.95	$2.62 \pm 0.05$	$1.80 \pm 0.12$	1.12	blue asy
LkHA 208	$-0.13 \pm 0.04$	$1.50 \pm 0.08$	1.30				$0.02 \pm 0.03$	$1.87 \pm 0.07$	3.01	$-0.04 \pm 0.04$	$1.21 \pm 0.13$	2.53	two comp
LkHA 339	$11.57 \pm 0.02$	$3.08 \pm 0.04$	2.97	$11.03 \pm 0.06$	$2.27 \pm 0.14$	2.49							self-abs
LkHA 215	$2.67 \pm 0.02$	$1.96 \pm 0.05$	1.70	$2.34 \pm 0.03$	$1.10 \pm 0.07$	2.10	$2.82 \pm 0.02$	$2.55 \pm 0.04$	6.62	$2.89 \pm 0.05$	$2.48 \pm 0.13$	7.62	red-asy
R Mon	$9.55 \pm 0.04$	$1.57 \pm 0.09$	0.61				$9.51 \pm 0.02$	$2.35 \pm 0.06$	4.10	$9.69 \pm 0.08$	$1.93 \pm 0.07$	3.80	red-asy
V590 Mon	$5.48 \pm 0.04$	$1.75 \pm 0.09$	0.72	$4.96 \pm 0.12$	$3.00 \pm 0.34$	0.84	$5.06 \pm 0.03$	$3.25 \pm 0.06$	2.41				three comp
	$9.02 \pm 0.05$	$1.61 \pm 0.13$	0.68	$8.76 \pm 0.10$	$1.74 \pm 0.22$	0.83	$8.93 \pm 0.01$	$2.02 \pm 0.02$	6.37	$8.95 \pm 0.04$	$1.93 \pm 0.10$	6.74	
	$11.48 \pm 0.06$	$1.78 \pm 0.20$	0.56	$11.38 \pm 0.05$	$1.31 \pm 0.15$	1.33	$11.45 \pm 0.01$	$1.58 \pm 0.02$	4.99	$11.53 \pm 0.04$	$1.52 \pm 0.09$	5.87	
VV Ser							5.34	$1.73 \pm 0.04$	1.14	$5.38 \pm 0.29$	$1.43 \pm 0.29$	0.77	three comp
							$7.32 \pm 0.01$	$1.91 \pm 0.04$	1.29	$7.53 \pm 0.29$	$1.73 \pm 0.29$	1.92	
							$9.51 \pm 0.01$	$2.08 \pm 0.04$	0.92	$9.13 \pm 0.29$	$1.47 \pm 0.29$	0.81	
MWC 300							$6.54 \pm 0.21$	$2.12 \pm 0.21$	0.42	$6.48 \pm 0.13$	$0.55 \pm 0.21$	0.21	three comp?
							$8.27 \pm 0.21$	$1.87 \pm 0.21$	1.15	$7.92 \pm 0.06$	$1.44 \pm 0.20$	0.85	
							$10.12 \pm 0.21$	$1.62 \pm 0.21$	1.24	$10.00 \pm 0.08$	$1.70 \pm 0.19$	0.76	
AS 310							$7.07 \pm 0.07$	$2.15 \pm 0.13$	0.53	$7.28 \pm 0.20$	$1.90 \pm 0.87$	0.54	
MWC 614							$2.22 \pm 0.09$	$1.10 \pm 0.20$	0.39				
Par 21							$16.79 \pm 0.04$	$1.07 \pm 0.09$	0.66	$16.97 \pm 0.07$	$0.81 \pm 0.15$	0.82	
V1685 Cyg	$7.61 \pm 0.02$	$1.90 \pm 0.05$	5.22	$7.79 \pm 0.03$	$1.89 \pm 0.07$	6.60	$7.59 \pm 0.02$	$2.83 \pm 0.06$	9.98	$7.60 \pm 0.07$	$2.68 \pm 0.22$	9.83	two comp
							$12.64 \pm 0.08$	$3.27 \pm 0.19$	2.86				
Par 22							4.84	$3.17 \pm 0.02$	8.04	$5.00 \pm 0.02$	$2.90 \pm 0.04$	7.69	two comp?
							$9.21 \pm 0.03$	$2.90 \pm 0.06$	1.61	$9.51 \pm 0.11$	$3.14 \pm 0.33$	1.34	

Table 2—Continued

Name	<sup>13</sup> CO (2-1)			<sup>13</sup> CO (3-2)			CO (2-1)			CO (3-2)			Notes
	V <sub>LSR</sub> (km s <sup>-1</sup> )	FWHM (km s <sup>-1</sup> )	T <sub>A</sub> <sup>*</sup> (K)	V <sub>LSR</sub> (km s <sup>-1</sup> )	FWHM (km s <sup>-1</sup> )	T <sub>A</sub> <sup>*</sup> (K)	V <sub>LSR</sub> (km s <sup>-1</sup> )	FWHM (km s <sup>-1</sup> )	T <sub>A</sub> <sup>*</sup> (K)	V <sub>LSR</sub> (km s <sup>-1</sup> )	FWHM (km s <sup>-1</sup> )	T <sub>A</sub> <sup>*</sup> (K)	
PV Cep	2.78 ± 0.07	0.66 ± 0.16	0.72				2.15 ± 0.03	2.98 ± 0.06	1.97				red asy
AS 442	0.14 ± 0.04	1.12 ± 0.09	0.77				0.23 ± 0.01	1.44 ± 0.04	3.14	0.22 ± 0.03	1.43 ± 0.09	3.29	red wing
LkHA 134							0.70 ± 0.02	1.79 ± 0.04	2.15	0.94 ± 0.03	1.28 ± 0.08	1.89	
HD 200775	2.30 ± 0.02	1.90 ± 0.05	1.49	2.66 ± 0.14	2.68 ± 0.38	0.95	1.68 ± 0.01	3.53 ± 0.01	4.71	1.60 ± 0.03	3.18 ± 0.06	4.91	blue asy
LkHA 324							-2.43 ± 0.03	5.62 ± 0.07	3.36	-2.17 ± 0.04	5.13 ± 0.09	3.96	blue asy?
V645 Cyg	-44.05 ± 0.07	2.94 ± 0.15	1.96	-43.52 ± 0.10	1.45 ± 0.19	3.89	-44.07 ± 0.03	3.87 ± 0.07	3.64	-43.88 ± 0.03	2.88 ± 0.07	4.93	
LkHA 234	-10.40 ± 0.01	2.15 ± 0.02	5.14	-10.55 ± 0.03	1.98 ± 0.08	6.71	-10.11 ± 0.02	3.85 ± 0.05	10.58	-10.11 ± 0.02	2.94 ± 0.05	10.21	red wing?
AS 477							6.54 ± 0.01	2.74 ± 0.04	3.83	6.66 ± 0.03	2.12 ± 0.10	4.41	red asy?
BD46	6.25 ± 0.02	1.39 ± 0.05	2.21	6.89 ± 0.07	1.21 ± 0.16	2.37	6.70 ± 0.01	2.30 ± 0.04	3.54	6.71 ± 0.03	1.97 ± 0.07	3.44	blue wing
BH Cep							1.81 ± 0.07	0.93 ± 0.16	0.35				
V375 Lac							-0.18	1.72 ± 0.01	7.13	-0.28	1.55 ± 0.01	9.90	
IL Cep	-9.99 ± 0.03	1.78 ± 0.08	1.62				-10.13 ± 0.04	2.95 ± 0.09	1.72	-9.95 ± 0.09	2.10 ± 0.24	0.83	flat top
MWC 1080	-30.52 ± 0.02	4.47 ± 0.06	1.91	-30.52 ± 0.05	3.48 ± 0.14	1.46							red profile,wings
LkHA 259	-7.13 ± 0.06	1.98 ± 0.13	1.17	-6.04 ± 0.07	1.45 ± 0.17	2.27							blue profile

Table 3. Derived parameters of the lines

Name	$V_{LSR}$ (km s <sup>-1</sup> )	$\frac{12_{co(2-1)}}{13_{co(2-1)}}$	$\tau_{13co(2-1)}$	$\tau_{12co(2-1)}$	$T_{ex}$ (K)	$\Theta_s$ ( $''$ )	$\frac{12_{co(3-2)}}{12_{co(2-1)}}$	$N_{H_2}$ (10 <sup>21</sup> cm <sup>-2</sup> )
MacC H12	-4.7	3.6	0.33	28.96	20.93	179	0.95	5.49
LkHA 198	-0.2	3.1	0.39	34.66	15.76	530	0.68	5.89
RNO 6	-36.0	2.8	0.44	39.32	10.20	230	0.77	3.06
XY Per	-4.2	7.4	0.15	12.92	11.24	133	0.64	1.55
V892 Tau	7.2	4.2	0.27	24.20	12.05	310	0.64	2.76
AB Aur	6.1			26.60	15.29	188	0.72	1.40
T Ori	7.5	4.4	0.26	22.95	86.79	74	0.87	39.81
	11.0	6.4	0.17	15.12	44.65	141	0.87	13.47
	13.2	8.9	0.12	10.61	32.99	162	0.92	6.16
V380 Ori	7.0			26.60				
	9.0	2.2	0.61	53.95	16.36	800	0.69	12.83
V586 Ori	6.5			26.60	8.36	300	0.72	1.23
	8.7			26.60	24.12	153	0.82	3.68
BF Ori	6.2	4.1	0.28	24.88	17.12	285	0.72	4.42
	9.2	3.4	0.35	31.00	14.57	164	1.00	3.59
	10.9	2.6	0.49	43.21	7.55	300	0.54	1.66
Haro 13A	5.6	4.3	0.26	23.56	14.25	600	0.68	4.11
V599 Ori	5.0	5.2	0.21	19.01	11.43		0.70	2.66
	7.2			26.60				
RR Tau	-5.4	4.5	0.25	22.37	21.09	126	0.90	3.43
V350 Ori	4.4	6.3	0.17	15.38	6.84		0.60	1.20
MWC 789	2.6	3.8	0.31	27.18	7.06		0.50	1.33
LkHA 208	-0.1	2.9	0.42	37.63	10.05	290	0.45	2.28
LkHA 339	11.3	3.8	0.31	27.18	> 12.7			> 7.53
LkHA 215	2.5	5.1	0.22	19.42	20.66	170	0.86	4.08
R Mon	9.6	10.1	0.10	9.28	12.58	250	0.61	0.91
V590 Mon	5.2	6.2	0.18	15.65	10.16			1.08
	8.9	11.8	0.09	7.88	18.24	207	0.83	1.09
	11.4	7.9	0.14	12.05	17.88	152	0.82	1.26
VV Ser	5.4			26.60	6.23	270	0.44	0.98
	7.4			26.60	12.69	74	0.71	2.04

Table 3—Continued

Name	$V_{LSR}$ (km s <sup>-1</sup> )	$\frac{^{12}co(2-1)}{^{13}co(2-1)}$	$\tau_{13co(2-1)}$	$\tau_{12co(2-1)}$	$T_{ex}$ (K)	$\Theta_s$ ( $''$ )	$\frac{^{12}co(3-2)}{^{12}co(2-1)}$	$N_{H_2}$ (10 <sup>21</sup> cm <sup>-2</sup> )
	9.3			26.60	6.81	140	0.43	1.25
MWC 300	6.5			26.60	4.32	300	0.09	1.00
	8.1			26.60	6.53	220	0.51	1.08
	10.1			26.60	6.08	500	0.58	0.91
AS 310	7.2			26.60	6.47	95	0.55	1.24
MWC 614	2.2			26.60	4.56			0.35
Par 21	16.9			26.60	8.18	78	0.50	0.74
V1685 Cyg	7.7	2.8	0.44	39.32	22.23	330	0.83	10.00
	12.6			26.60	11.26			2.00
Par 22	4.9			26.60	18.75	340	0.83	5.64
	9.4			26.60	7.84	200	0.74	1.92
PV Cep	2.8	12.4	0.08	7.48	9.05			0.43
AS 442	0.1	5.2	0.21	19.01	12.40	165	0.77	1.11
LkHA 134	0.8			26.60	9.07	205	0.50	1.34
HD 200775	2.5	5.9	0.19	16.53	15.13	193	0.73	3.08
LkHA 324	-2.3			26.60	14.55	135	0.71	7.11
V645 Cyg	-43.8	2.4	0.54	47.97	18.13	109	0.65	12.32
LkHA 234	-10.5	3.7	0.32	28.04	22.56	390	0.66	10.13
AS477/BD46	6.6	2.7	0.46	41.17	15.10	147	0.59	4.68
BH Cep	1.8			26.60	4.41			0.29
V375 Lac	-0.2			26.60	28.38	119	0.81	5.76
IL Cep	-10.0	1.8	0.81	72.17	6.51		0.30	5.34
MWC 1080	-30.5			26.60	> 11.8			> 7.19
LkHA 259	-6.6			26.60	> 6.4			> 3.49

Table 4. The SED fitting results

Name	$A_V$ (mag)	$\log(\text{Age})$ $\log(\text{yr})$	$M_*$ ( $M_\odot$ )	$R_*$ ( $R_\odot$ )	$\log(L_*)$ $\log(L_\odot)$	$\log(T_*)$ $\log(\text{K})$	$\log(M_{env})$ $\log(M_\odot)$	$\log\dot{M}_{env}$ $\log(M_\odot \text{yr}^{-1})$	$\log(M_{disk})$ $\log(M_\odot)$	Incl ( $^\circ$ )	$\log(R_{out})$ $\log(\text{AU})$	$\log(\dot{M}_{disk})$ $\log(M_\odot \text{yr}^{-1})$
MacC H12	$0.61 \pm 0.57$	$3.73 \pm 0.32$	$1.84 \pm 0.16$	$14.96 \pm 2.44$	$1.79 \pm 0.13$	3.62	$0.32 \pm 0.16$	$-4.88 \pm 0.07$	$-1.74 \pm 0.10$	18.19	$1.21 \pm 0.32$	$-6.55 \pm 0.35$
LkHA 198	0.00	$3.07 \pm 0.06$	$3.84 \pm 0.38$	$29.95 \pm 5.60$	$2.42 \pm 0.14$	3.62	$0.06 \pm 0.35$	$-4.56 \pm 0.13$	$-2.12 \pm 0.63$	$57.17 \pm 24.78$	$0.54 \pm 0.16$	$-5.33 \pm 0.12$
Vx Cas	$1.48 \pm 0.30$	$6.66 \pm 0.25$	$3.62 \pm 0.24$	$2.22 \pm 0.08$	$2.17 \pm 0.11$	$4.13 \pm 0.02$	$-4.30 \pm 0.54$		$-2.55 \pm 0.13$	$41.80 \pm 19.87$	$3.00 \pm 0.32$	$-7.89 \pm 0.46$
RNO 6	$0.71 \pm 0.65$	$6.03 \pm 0.07$	$5.10 \pm 0.42$	$2.76 \pm 0.08$	$2.75 \pm 0.12$	$4.23 \pm 0.02$	$1.08 \pm 0.10$	$-8.47 \pm 0.31$	$-1.78 \pm 0.23$	$78.59 \pm 2.92$	$2.40 \pm 0.21$	$-6.79 \pm 0.94$
IP Per	$0.00 \pm 0.01$	$5.71 \pm 0.09$	$2.17 \pm 0.47$	$5.03 \pm 0.50$	$1.09 \pm 0.09$	$3.67 \pm 0.01$	$-1.64 \pm 0.44$	$-5.62 \pm 0.41$	$-1.49 \pm 0.35$	$28.66 \pm 9.47$	$2.45 \pm 0.25$	$-6.85 \pm 0.78$
V892 Tau	$6.44 \pm 1.95$	$6.50 \pm 0.37$	$2.50 \pm 0.88$	$4.04 \pm 2.84$	$1.81 \pm 0.24$	$3.98 \pm 0.18$	$-0.88 \pm 0.38$	$-5.62 \pm 0.38$	$-1.29 \pm 0.30$	$30.50 \pm 9.53$	$2.69 \pm 0.35$	$-7.14 \pm 0.15$
XY Per	$3.06 \pm 0.09$	6.99	2.81	1.93	1.75	4.06	-5.71		-2.02	$78.61 \pm 2.92$	2.77	-8.81
AB Aur	1.04	5.14	1.10	6.73	1.10	3.62	-1.33	-5.65	-2.12	31.79	2.15	-7.34
MWC 480	$0.33 \pm 0.35$	$6.33 \pm 0.16$	$3.04 \pm 0.33$	$4.47 \pm 1.10$	$1.78 \pm 0.92$	$3.86 \pm 0.19$	$-6.13 \pm 0.35$		$-1.29 \pm 0.25$	$54.75 \pm 19.35$	$2.38 \pm 0.25$	$-6.36 \pm 0.67$
HD 35929	$0.24 \pm 0.16$	$6.36 \pm 0.19$	$3.10 \pm 0.47$	$5.19 \pm 0.95$	$1.81 \pm 0.23$	$3.85 \pm 0.03$	$-2.87 \pm 0.36$		$-4.87 \pm 0.63$	$56.30 \pm 19.64$	$3.61 \pm 0.72$	$-10.66 \pm 0.71$
HD 36112	$0.60 \pm 0.04$	$6.96 \pm 0.05$	$1.95 \pm 0.05$	$1.83 \pm 0.05$	$1.11 \pm 0.02$	3.91	$-5.86 \pm 0.44$		$-1.78 \pm 0.49$	$35.05 \pm 11.45$	$2.58 \pm 0.33$	$-8.23 \pm 0.14$
HD 245185	0.00	6.13	3.74	5.68	2.17	3.93	-6.84		-1.41	81.37	2.29	-7.19
T Ori	$1.47 \pm 0.16$	$6.69 \pm 0.28$	$3.72 \pm 0.51$	$2.33 \pm 0.31$	$2.27 \pm 0.18$	$4.13 \pm 0.04$	$-5.42 \pm 0.46$		$-1.26 \pm 0.51$	$53.80 \pm 15.54$	$2.60 \pm 0.71$	$-6.54 \pm 0.43$
CQ Tau	$2.31 \pm 0.13$	$6.85 \pm 0.15$	$2.82 \pm 0.27$	$2.07 \pm 0.03$	$1.78 \pm 0.16$	$4.04 \pm 0.04$	$-4.50 \pm 0.32$		$-2.03 \pm 0.47$	$47.41 \pm 31.50$	$2.67 \pm 0.23$	$-7.47 \pm 0.54$
V380 Ori	$2.87 \pm 1.42$	$5.87 \pm 0.11$	$4.68 \pm 0.05$	$6.62 \pm 2.95$	$2.62 \pm 0.21$	$4.03 \pm 0.13$	$0.88 \pm 0.21$	$-5.66 \pm 0.43$	$-3.51 \pm 0.29$	$45.12 \pm 18.54$	$2.88 \pm 0.39$	$-8.52 \pm 0.48$
V586 Ori	1.00	6.01	3.86	7.62	1.93	3.80	-0.06	-7.56	-1.60	81.37	2.24	-6.86
BF Ori	$1.81 \pm 0.31$	$6.72 \pm 0.17$	$3.09 \pm 0.31$	$2.19 \pm 0.29$	$1.94 \pm 0.16$	$4.07 \pm 0.04$	$-4.60 \pm 0.98$		$-2.94 \pm 0.57$	$49.03 \pm 21.24$	$2.58 \pm 0.53$	$-8.08 \pm 0.59$
HD37411	11.65	6.63	0.35	1.04	-0.15	3.55	-8.77		-2.33	63.26	2.09	-7.18
Haro 13A	0.00	3.02	3.47	24.48	$1.34 \pm 0.32$	3.63	$-0.25 \pm 0.65$	-4.71	-1.84	$64.16 \pm 21.08$	0.67	$-5.62 \pm 0.36$
V599 Ori	$2.94 \pm 1.62$	$5.64 \pm 0.30$	$1.83 \pm 1.19$	$5.29 \pm 1.59$	$1.20 \pm 0.31$	$3.65 \pm 0.06$	$-1.36 \pm 0.52$	$-5.76 \pm 0.35$	$-1.24 \pm 0.27$	$42.47 \pm 24.22$	$2.59 \pm 0.46$	$-6.71 \pm 0.37$
RR Tau	$1.82 \pm 0.27$	$6.53 \pm 0.28$	$3.68 \pm 0.42$	$2.60 \pm 0.49$	$2.30 \pm 0.17$	$4.12 \pm 0.03$	$-5.71 \pm 0.46$		$-1.12 \pm 0.24$	$43.72 \pm 19.52$	$2.60 \pm 0.32$	$-6.41 \pm 0.32$
V350 Ori	$1.69 \pm 0.47$	$6.73 \pm 0.16$	$2.73 \pm 0.39$	$2.05 \pm 0.31$	$1.75 \pm 0.19$	$4.03 \pm 0.06$	$-3.48 \pm 0.39$		$-2.52 \pm 0.50$	$43.21 \pm 19.30$	$3.39 \pm 0.32$	$-7.29 \pm 0.73$
MWC 789	$2.42 \pm 0.77$	$6.24 \pm 0.17$	$3.90 \pm 0.37$	$2.81 \pm 0.29$	$2.36 \pm 0.10$	$4.12 \pm 0.02$	$-6.47 \pm 0.18$		$-1.02 \pm 0.13$	$22.65 \pm 6.39$	$2.43 \pm 0.05$	$-6.49 \pm 0.37$



Table 4—Continued

Name	$A_v$ (mag)	$\log(\text{Age})$ $\log(\text{yr})$	$M_*$ ( $M_\odot$ )	$R_*$ ( $R_\odot$ )	$\log(L_*)$ $\log(L_\odot)$	$\log(T_*)$ $\log(\text{K})$	$\log(M_{env})$ $\log(M_\odot)$	$\log\dot{M}_{env}$ $\log(M_\odot\text{yr}^{-1})$	$\log(M_{disk})$ $\log(M_\odot)$	Incl ( $^\circ$ )	$\log(R_{out})$ $\log(\text{AU})$	$\log(\dot{M}_{disk})$ $\log(M_\odot\text{yr}^{-1})$
LkHA 208	$5.39 \pm 0.09$	5.97	4.23	6.69	2.32	3.93	-0.93	-7.33	-1.00	$55.80 \pm 14.37$	3.06	-7.71
LkHA 339	$2.96 \pm 0.12$	$6.60 \pm 0.31$	$3.42 \pm 0.60$	$2.25 \pm 0.25$	$2.17 \pm 0.28$	$4.11 \pm 0.05$	$-2.38 \pm 0.76$		$-1.78 \pm 0.36$	$40.20 \pm 21.08$	$3.73 \pm 0.52$	$-8.67 \pm 0.38$
LkHA 215	$1.34 \pm 0.35$	5.74	5.13	8.46	2.59	3.95	1.05	-5.01	-2.15	$46.40 \pm 21.09$	3.65	-9.19
R Mon	4.87	4.24	4.67	24.59	2.29	3.64	-0.61	-4.56	-1.95	18.19	1.55	-6.97
V590 Mon	$0.42 \pm 0.15$	$6.45 \pm 0.54$	$4.71 \pm 0.20$	$5.86 \pm 3.12$	$2.47 \pm 0.04$	$4.06 \pm 0.15$	$-1.86 \pm 0.68$	$-6.57 \pm 0.73$	$-2.25 \pm 0.31$	$84.45 \pm 2.87$	$3.03 \pm 0.36$	$-8.03 \pm 0.31$
GU CMa	0.42	6.90	3.14	2.05	1.93	4.09	-3.51		-7.11	49.46	3.62	-13.76
HD 141569	$0.26 \pm 0.04$	6.93	2.14	1.74	1.33	3.97	-2.99		-4.81	$56.31 \pm 23.40$	3.72	-11.82
VV Ser	$3.98 \pm 0.25$	$6.81 \pm 0.20$	$3.32 \pm 0.35$	$2.16 \pm 0.15$	$2.10 \pm 0.18$	$4.10 \pm 0.03$	$-5.83 \pm 0.63$		$-1.39 \pm 0.31$	$45.71 \pm 15.48$	$2.72 \pm 0.28$	$-6.43 \pm 0.34$
MWC 300	$4.23 \pm 2.13$	$6.56 \pm 0.11$	$7.37 \pm 0.67$	$3.33 \pm 0.19$	$3.35 \pm 0.13$	$4.33 \pm 0.03$	$-6.44 \pm 0.38$		$-1.05 \pm 0.01$	$62.27 \pm 13.03$	$2.27 \pm 0.23$	$-5.80 \pm 0.80$
AS 310	$6.65 \pm 3.01$	$5.85 \pm 0.21$	$9.86 \pm 0.53$	$3.90 \pm 0.10$	$3.79 \pm 0.09$	$4.41 \pm 0.01$	$1.61 \pm 0.08$	$-4.31 \pm 0.9$	$-0.59 \pm 0.11$	87.13	$3.26 \pm 0.44$	$-5.53 \pm 0.80$
Par 21	1.61	6.13	3.74	5.68	2.17	3.93	-6.84		-1.41	87.13	2.29	-7.19
V1295 Aql	0.36	$6.69 \pm 0.30$	$3.22 \pm 0.37$	$2.29 \pm 0.34$	$2.00 \pm 0.18$	$4.07 \pm 0.01$	$-6.67 \pm 0.30$		$-2.55 \pm 0.31$	$66.45 \pm 9.44$	$1.55 \pm 0.09$	$-7.18 \pm 0.53$
V1685 Cyg	$1.35 \pm 0.95$	$4.93 \pm 0.37$	$6.75 \pm 1.40$	$24.50 \pm 12.49$	$3.08 \pm 0.14$	$3.85 \pm 0.13$	$1.30 \pm 0.24$	$-4.08 \pm 0.32$	$-1.04 \pm 0.35$	$35.64 \pm 14.64$	$1.74 \pm 0.34$	$-4.61 \pm 0.38$
Par 22	$3.67 \pm 2.57$	$5.35 \pm 0.35$	$1.29 \pm 1.14$	$6.46 \pm 2.88$	$1.24 \pm 0.34$	$3.59 \pm 0.09$	$-0.06 \pm 0.48$	$-4.21 \pm 0.55$	$-1.71 \pm 0.35$	$54.82 \pm 29.65$	$2.00 \pm 1.47$	$-6.35 \pm 0.52$
PV Cep	$3.16 \pm 0.43$	$3.08 \pm 0.06$	$0.28 \pm 0.09$	$5.69 \pm 0.25$	$1.77 \pm 0.18$	$3.51 \pm 0.03$	$-0.49 \pm 0.19$	$-5.33 \pm 0.06$	$-1.53 \pm 0.34$	18.19	$0.30 \pm 0.16$	$-4.40 \pm 0.06$
AS 442	$1.98 \pm 0.24$	$6.54 \pm 0.22$	$4.31 \pm 0.37$	$2.67 \pm 0.60$	$2.48 \pm 0.15$	$4.17 \pm 0.04$	$-3.41 \pm 0.61$		$-1.99 \pm 0.39$	$55.67 \pm 13.68$	$2.92 \pm 0.45$	$-6.99 \pm 0.47$
LkHA 134	$2.67 \pm 0.11$	$6.27 \pm 0.13$	$4.13 \pm 0.31$	$2.67 \pm 0.36$	$2.45 \pm 0.14$	$4.16 \pm 0.02$	$-2.07 \pm 0.06$	$-8.05 \pm 0.50$	$-1.75 \pm 0.26$	$58.33 \pm 20.25$	$3.90 \pm 0.20$	$-9.06 \pm 0.52$
HD 200775	$0.12 \pm 0.08$	$5.34 \pm 0.01$	$6.65 \pm 0.09$	$14.22 \pm 0.06$	$2.78 \pm 0.03$	$3.88 \pm 0.01$	$1.61 \pm 0.05$	$-3.59 \pm 0.30$	$-2.33 \pm 0.01$	$26.17 \pm 11.03$	$1.93 \pm 0.12$	$-7.86 \pm 0.11$
LkHA 324	$1.01 \pm 1.09$	$6.16 \pm 1.27$	$2.32 \pm 0.77$	$4.87 \pm 1.24$	$1.47 \pm 0.43$	$3.76 \pm 0.20$	$-1.50 \pm 0.51$	$-5.54 \pm 0.42$	$-1.89 \pm 0.45$	$41.68 \pm 19.41$	$2.67 \pm 0.97$	$-7.74 \pm 0.56$
HD 203024	$0.45 \pm 0.30$	$6.89 \pm 0.07$	$2.35 \pm 0.15$	$1.89 \pm 0.06$	$1.48 \pm 0.09$	$3.99 \pm 0.03$	$-5.33 \pm 0.36$		$-2.06 \pm 0.02$	$74.29 \pm 4.39$	$2.27 \pm 0.26$	$-8.20 \pm 0.30$
V645 Cyg	0.42	5.16	10.59	4.16	3.88	4.42	2.46	-3.38	-2.26	18.19	2.96	-7.44
LkHA 234	$3.05 \pm 3.29$	$5.15 \pm 0.02$	$8.96 \pm 0.25$	$4.91 \pm 0.39$	$3.76 \pm 0.01$	$4.35 \pm 0.02$	$2.82 \pm 0.06$	$-2.97 \pm 0.05$	$-0.79 \pm 0.72$	$45.13 \pm 4.01$	$2.21 \pm 0.47$	$-5.34 \pm 1.02$
AS 477	$0.60 \pm 0.25$	$6.43 \pm 0.22$	$5.11 \pm 0.66$	$2.72 \pm 0.23$	$2.76 \pm 0.20$	$4.22 \pm 0.04$	$-5.86 \pm 0.45$		$-1.65 \pm 0.34$	$59.44 \pm 13.66$	$2.55 \pm 0.36$	$-6.27 \pm 0.35$

Table 4—Continued

Name	$A_V$ (mag)	$\log(\text{Age})$ $\log(\text{yr})$	$M_*$ ( $M_\odot$ )	$R_*$ ( $R_\odot$ )	$\log(L_*)$ $\log(L_\odot)$	$\log(T_*)$ $\log(\text{K})$	$\log(M_{env})$ $\log(M_\odot)$	$\log\dot{M}_{env}$ $\log(M_\odot\text{yr}^{-1})$	$\log(M_{disk})$ $\log(M_\odot)$	Incl ( $^\circ$ )	$\log(R_{out})$ $\log(\text{AU})$	$\log(\dot{M}_{disk})$ $\log(M_\odot\text{yr}^{-1})$
LkHA 257	$2.62 \pm 0.83$	$6.62 \pm 0.16$	$3.61 \pm 0.64$	$2.68 \pm 1.60$	$2.18 \pm 0.16$	$4.11 \pm 0.09$	$-2.31 \pm 0.66$	$-6.99 \pm 0.70$	$-2.46 \pm 0.71$	$57.05 \pm 22.40$	$3.43 \pm 0.34$	$-7.14 \pm 0.71$
BH Cep	$0.80 \pm 0.34$	$6.61 \pm 0.29$	$3.27 \pm 0.21$	$3.35 \pm 1.33$	$2.05 \pm 0.13$	$4.03 \pm 0.06$	$-3.49 \pm 0.33$		$-2.50 \pm 0.70$	$84.26 \pm 2.88$	$3.53 \pm 0.14$	$-8.24 \pm 0.96$
SV Cep	$2.37 \pm 0.17$	$6.71 \pm 0.17$	$3.33 \pm 0.48$	$2.12 \pm 0.18$	$2.07 \pm 0.24$	$4.10 \pm 0.04$	$-6.40 \pm 0.54$		$-2.32 \pm 0.42$	$48.85 \pm 22.50$	$2.31 \pm 0.36$	$-7.55 \pm 0.68$
V375 Lac	$1.85 \pm 1.14$	$3.71 \pm 0.40$	$1.88 \pm 0.51$	$15.15 \pm 2.93$	$1.92 \pm 0.16$	$3.62 \pm 0.01$	$0.55 \pm 0.79$	$-4.45 \pm 0.15$	$-1.28 \pm 0.75$	18.19	$0.85 \pm 0.32$	$-5.18 \pm 0.48$
IL Cep	$0.28 \pm 0.32$	$6.02 \pm 0.10$	$3.85 \pm 0.19$	$7.53 \pm 1.07$	$1.94 \pm 0.15$	$3.81 \pm 0.07$	$-2.43 \pm 0.61$	$-7.08 \pm 0.54$	$-2.54 \pm 0.68$	$47.87 \pm 18.62$	$2.47 \pm 0.45$	$-8.25 \pm 0.34$
MWC 1080	$1.01 \pm 0.78$	$5.37 \pm 0.02$	$10.59 \pm 0.87$	$4.00 \pm 0.19$	$3.88 \pm 0.12$	$4.43 \pm 0.02$	$2.08 \pm 0.17$	$-3.58 \pm 0.21$	$-1.01 \pm 0.47$	$38.03 \pm 4.59$	$2.72 \pm 0.30$	$-5.92 \pm 0.37$
LkHA 259	$1.78 \pm 0.19$	$3.29 \pm 0.26$	$2.63 \pm 0.75$	$22.94 \pm 5.25$	$2.19 \pm 0.22$	3.61	$1.02 \pm 0.15$	$-3.09 \pm 0.14$	$-1.69 \pm 0.32$	18.19	$0.59 \pm 0.14$	$-5.50 \pm 0.28$

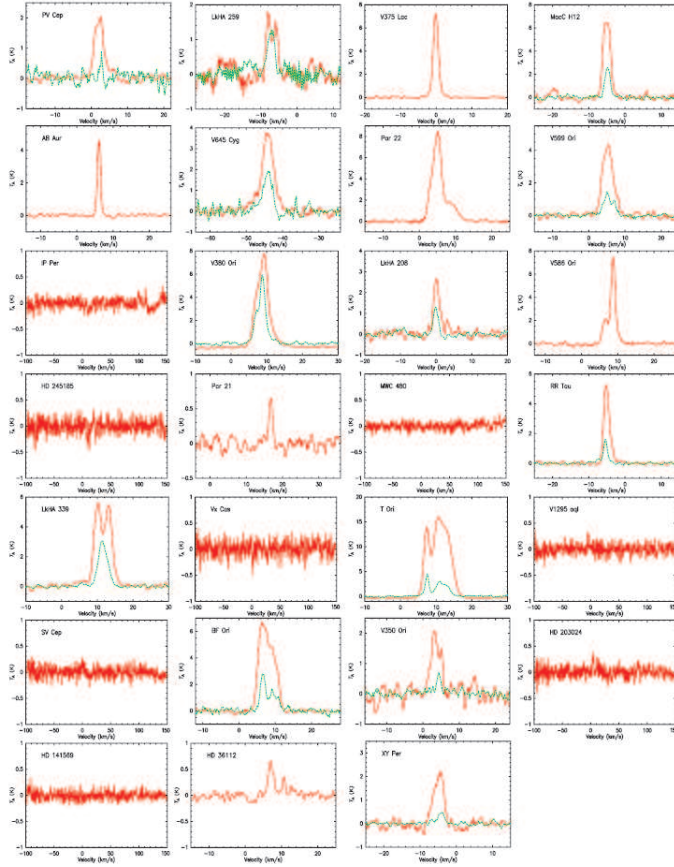


Fig. 1.—  $^{12}\text{CO}$  (2-1) (red) and  $^{13}\text{CO}$  (2-1) (green) lines of the A Type stars. The source names are plotted in the upper-left corner of each panel.

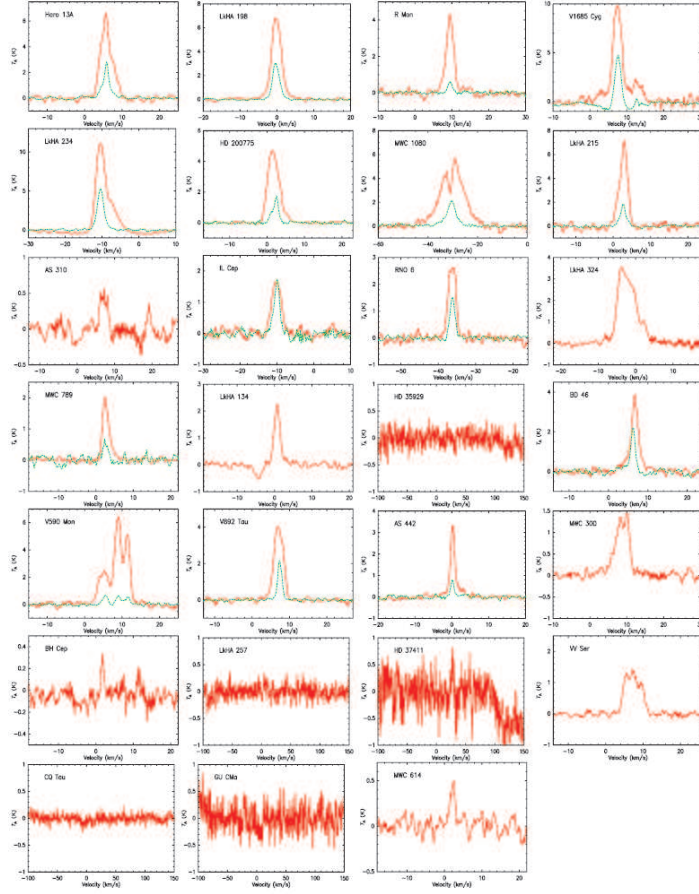


Fig. 2.—  $^{12}\text{CO}$  (2-1) (red) and  $^{13}\text{CO}$  (2-1) (green) lines of the B/F Type stars. The source names are plotted in the upper-left corner of each panel.

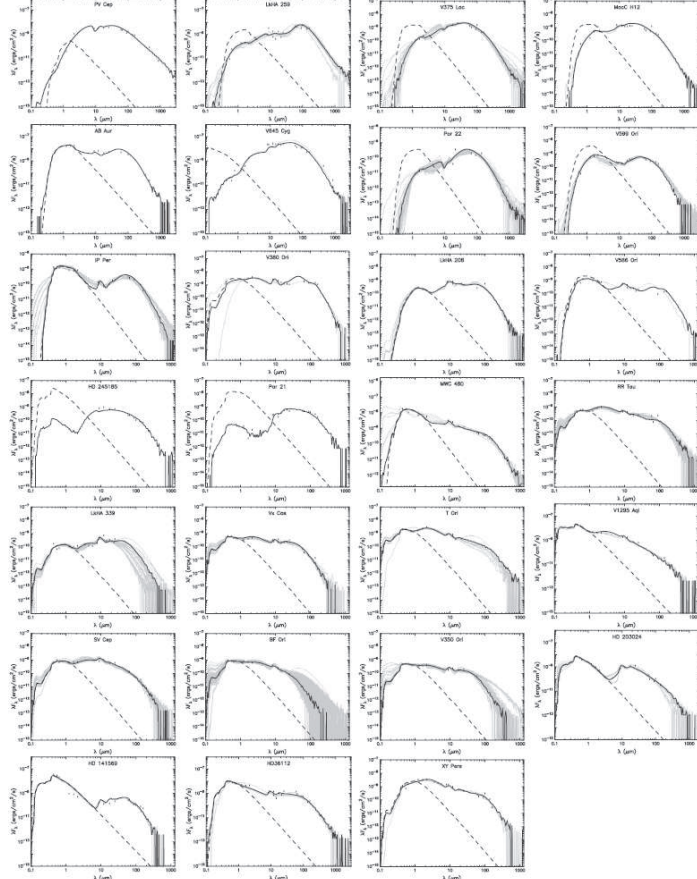


Fig. 3.— The SEDs of A Type stars. The observed data are plotted as circular symbols. The black solid line represents the best fit to the data, while the grey solid lines represent the fits with  $\chi^2 - \chi^2_{best} < 3 \times n_{data}$ . The dashed lines represent photospheric contributions, including the effect of foreground extinction, from the best-fitting models. As shown by the vertical lines, some model SEDs are with bad signal-to-noise ratios for wavelengths beyond 1-100  $\mu\text{m}$  (Robitaille et al. 2006).

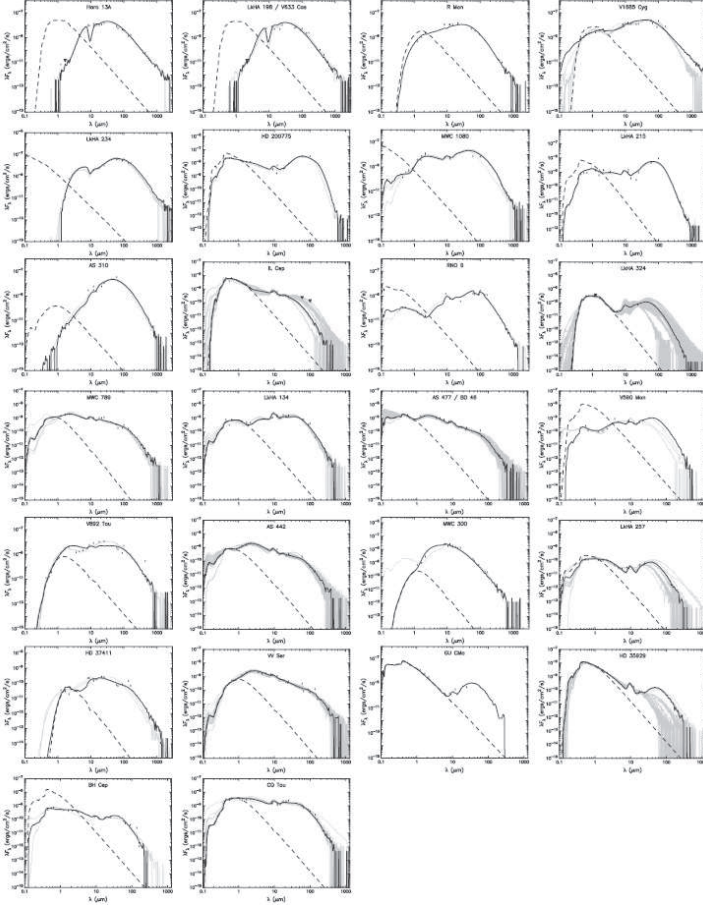


Fig. 4.— The SEDs of B/F Type stars. The symbols and lines are the same as in Fig.3

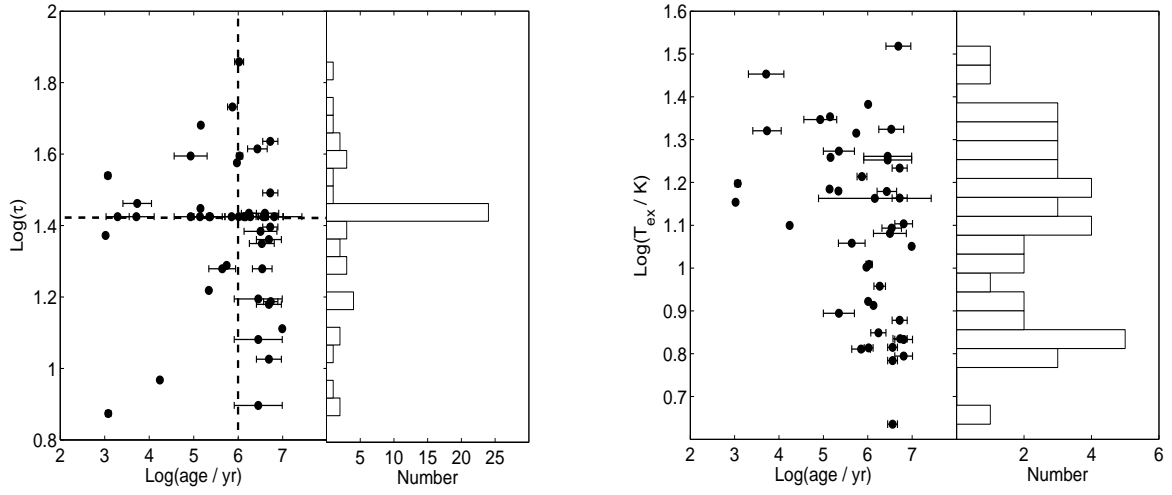


Fig. 5.— The optical depth  $\tau$  (left) of  $^{12}\text{CO}$  (2-1) and the excited temperature  $T_{\text{ex}}$  (right) as function of the age. The horizontal and vertical dashed lines in the left panel mark age at  $10^6$  yr and the average optical depth of 26.6.

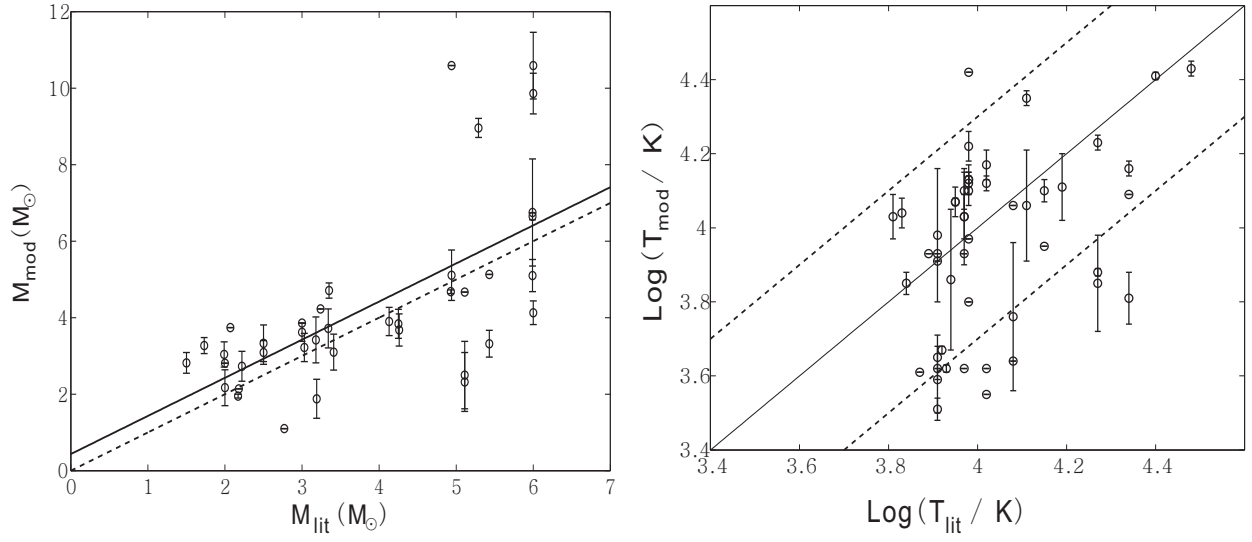


Fig. 6.— The masses derived from SED fitting compared to those obtained from Manoj et al. (2006) (left) and the effective temperatures of the stars obtained from SED fitting compared to the effective temperatures corresponding to the spectral types (right). The solid lines in both panels describe the least-square fitting. The dashed line in the left panel shows that  $M_{\text{mod}}$  is consistent with  $M_{\text{lit}}$ . The two dashed lines in the right panel mark out the area where the effective temperatures obtained from the two independent methods agree better than  $\pm 0.3$  orders of magnitude.



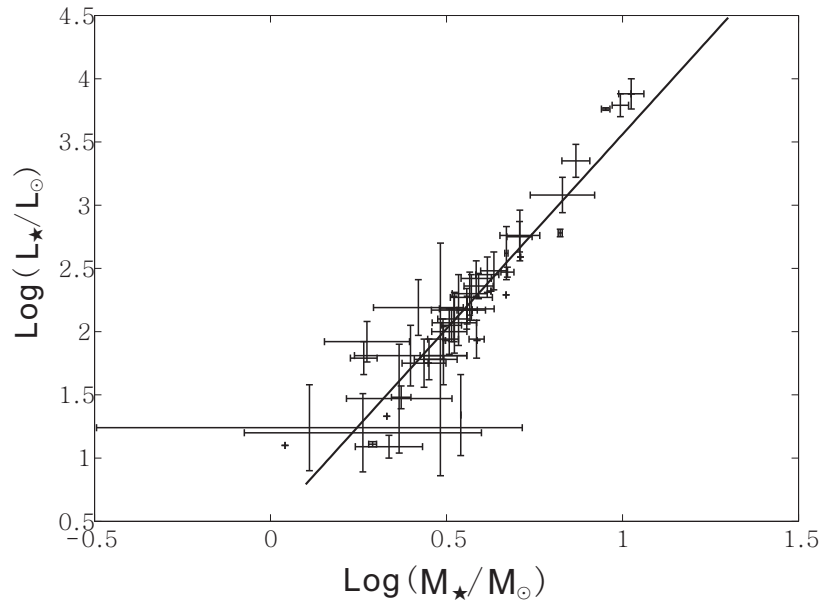


Fig. 7.— The mass-luminosity function of the sample stars. The solid line represents the best least-square fitting.

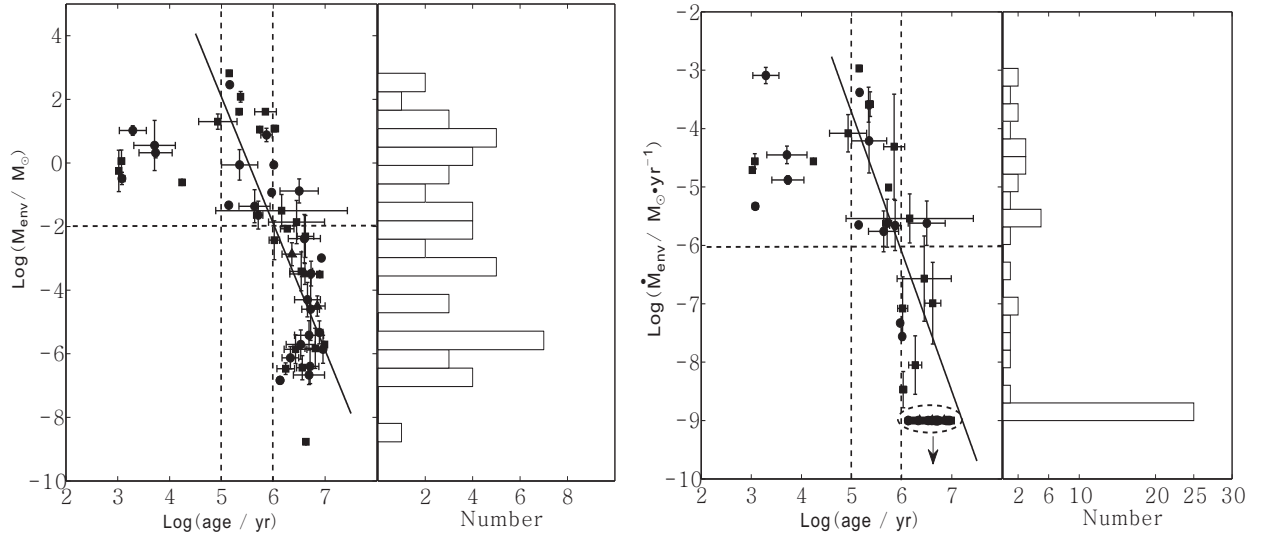


Fig. 8.— The envelope mass (left) and the envelope accretion rate (right) as function of the age. The solid lines represent the best least-square fitting. The vertical dashed lines mark age at  $10^5$  and  $10^6$  yr. The horizontal dashed line in the left and right panels mark the envelope mass of  $10^{-2} M_{\odot}$  and the envelope accretion rate of  $10^{-6} M_{\odot} \text{yr}^{-1}$ , respectively. The dashed oval in the right panel marks the sources with zero envelope accretion rate.

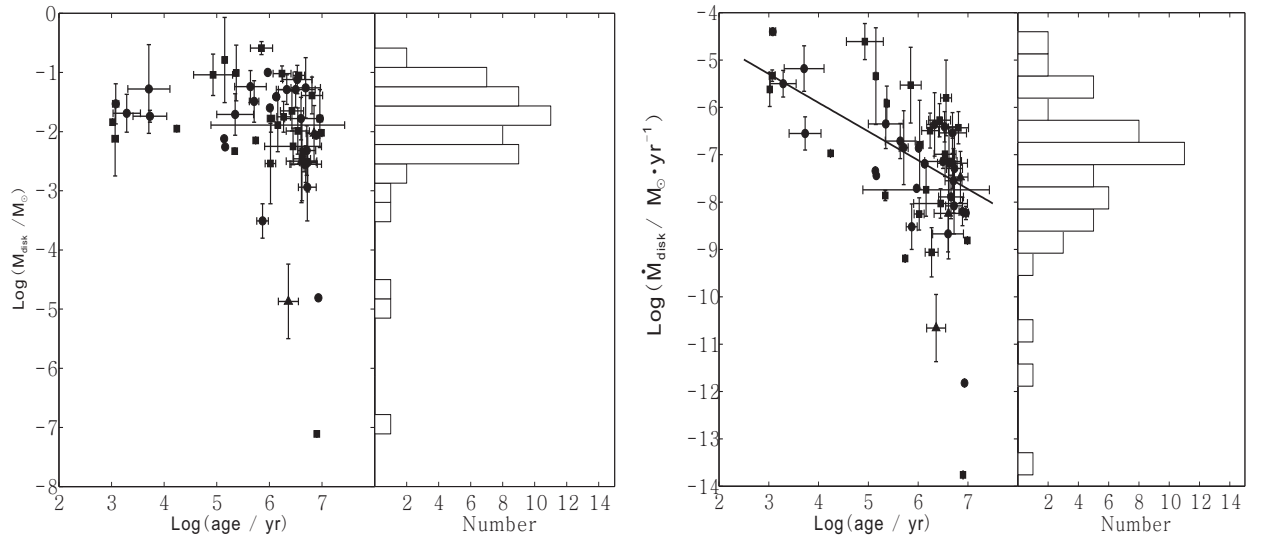


Fig. 9.— The disk mass (left) and the disk accretion rate (right) as function of the age. The solid lines represent the best least-square fitting.

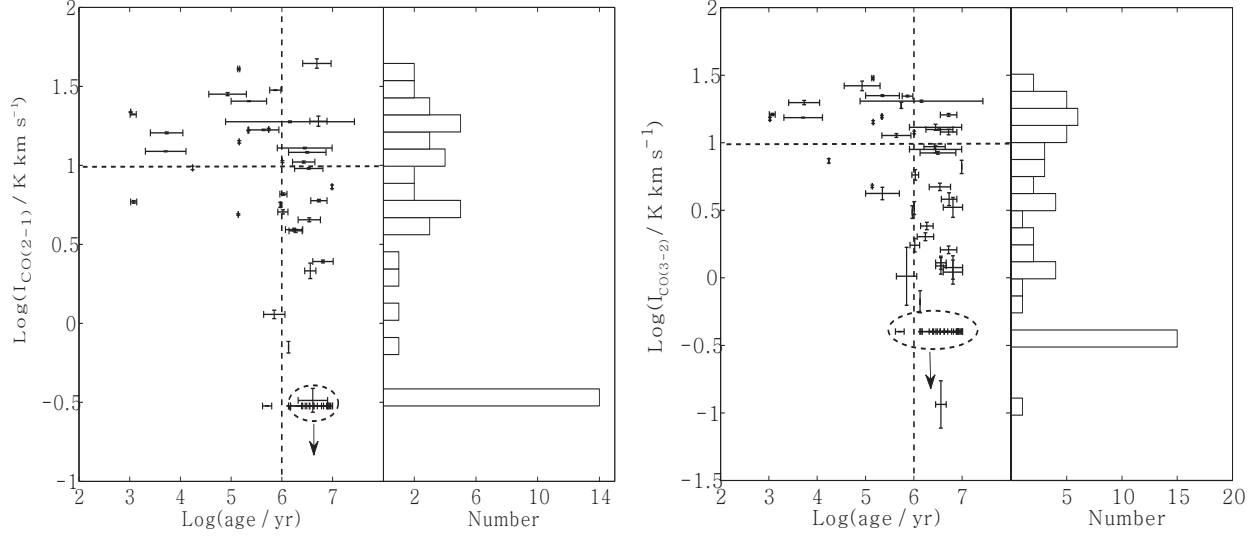


Fig. 10.— The  $^{12}\text{CO}$  (2-1) intensity (left) and the  $^{12}\text{CO}$  (3-2) intensity (right) as function of the age. The vertical and horizontal dashed lines are at age equalling  $10^6$  yr and  $^{12}\text{CO}$  intensity corresponding to  $10 \text{ K km s}^{-1}$ , respectively. The dashed ellipses encircle the sources with low signal-to-noise level in CO emission.

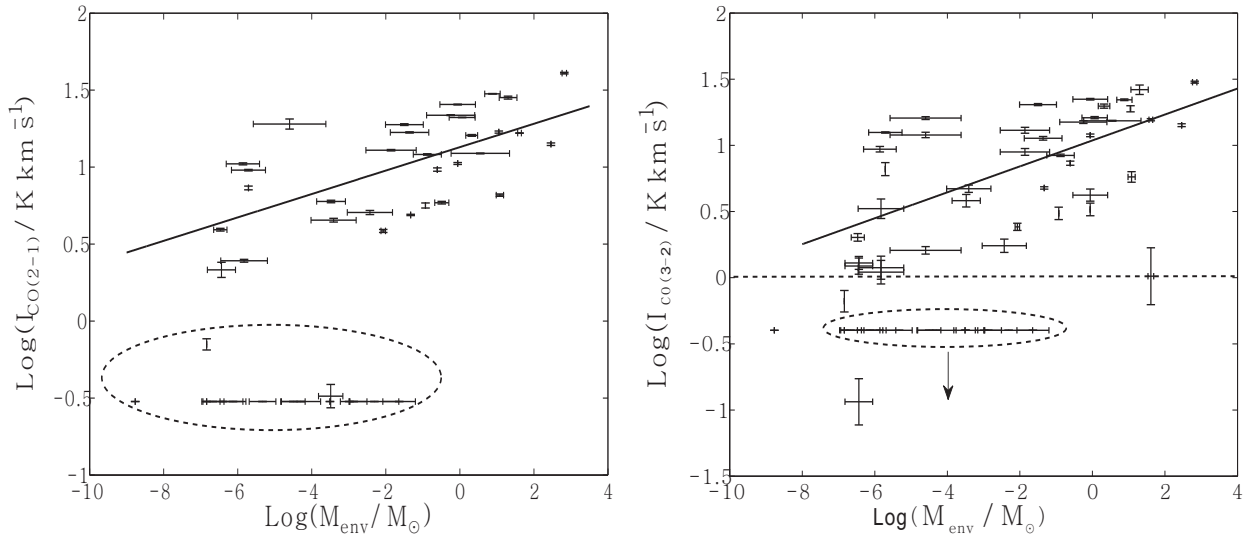


Fig. 11.— The  $^{12}\text{CO}$  (2-1) intensity (left) and the  $^{12}\text{CO}$  (3-2) intensity (right) as function of the envelope mass. The solid lines represent the best least-square fitting. The horizontal dashed line in the right panel is at where  $^{12}\text{CO}$  intensity corresponds to  $10 \text{ K km s}^{-1}$ . The sources with low signal-to-noise level in CO emission are shown in the dashed ellipses.